AMERICAN SOCIETY FOR MICROBIOLOGY | Molecular and Cellular Biology®

RESEARCH ARTICLE

Determining the Bioenergetic Capacity for Fatty Acid Oxidation in the Mammalian Nervous System

Cory J. White,[a] Jieun Lee,[a] Joseph Choi,[a] Tiffany Chu,[c] Susanna Scafidi,[c] Michael J. Wolfgang[a,b]

[a]Department of Biological Chemistry, Johns Hopkins School of Medicine, Baltimore, Maryland, USA
[b]Department of Pharmacology and Molecular Sciences, Johns Hopkins School of Medicine, Baltimore, Maryland, USA
[c]Department of Anesthesiology and Critical Care Medicine, Johns Hopkins School of Medicine, Baltimore, Maryland, USA

ABSTRACT The metabolic state of the brain can greatly impact neurologic function. Evidence of this includes the therapeutic benefit of a ketogenic diet in neurologic diseases, including epilepsy. However, brain lipid bioenergetics remain largely uncharacterized. The existence, capacity, and relevance of mitochondrial fatty acid β-oxidation (FAO) in the brain are highly controversial, with few genetic tools available to evaluate the question. We have provided evidence for the capacity of brain FAO using a pan-brain-specific conditional knockout (KO) mouse incapable of FAO due to the loss of carnitine palmitoyltransferase 2, the product of an obligate gene for FAO ($CPT2^{B-/-}$). Loss of central nervous system (CNS) FAO did not result in gross neuroanatomical changes or systemic differences in metabolism. Loss of CPT2 in the brain did not result in robustly impaired behavior. We demonstrate by unbiased and targeted metabolomics that the mammalian brain oxidizes a substantial quantity of long-chain fatty acids *in vitro* and *in vivo*. Loss of CNS FAO results in robust accumulation of long-chain acylcarnitines in the brain, suggesting that the mammalian brain mobilizes fatty acids for their oxidation, irrespective of diet or metabolic state. Together, these data demonstrate that the mammalian brain oxidizes fatty acids under normal circumstances with little influence from or on peripheral tissues.

KEYWORDS bioenergetics, brain, fatty acid, lipid, mitochondria, neurochemistry

The energy demands of the brain are thought to be overwhelmingly met by glucose. However, the brain can catabolize other substrates, most notably ketone bodies, which are produced using the final end products of mitochondrial fatty acid (FA) β-oxidation (FAO), which occurs primarily when glucose is limiting, such as during fasting or starvation (1). Neurologic dysfunction in humans is associated with impairments in FAO, including depression (2) and autism spectrum disorders (ASDs) (3–7). People with genetic disorders in FAO can also suffer from neurologic disorders, including encephalopathies, seizures, and cortical atrophy (8–10). Interestingly, dietary changes that increase circulating FAs, including a ketogenic (high-fat, low-carbohydrate) diet and intermittent fasting, can be used therapeutically (11). Furthermore, caloric restriction is associated with attenuation of symptoms of Parkinson's disease (12), and a high-fat diet (HFD) was beneficial in a mouse model of Huntington's disease (13, 14). Despite this evidence, the contributions of brain FA bioenergetics and the altered transcriptional imprint that occurs in response to metabolic cues, which when altered render the brain vulnerable to pathology, are not defined.

The brain is comprised of a unique composition of lipids compared to other tissues (15, 16). Astrocytes and neural stem cells express all the enzymes necessary for FAO, and the oxidation of radiolabeled FAs (17–20), [^{14}C]palmitate and [^{14}C]oleate, has been

Citation White CJ, Lee J, Choi J, Chu T, Scafidi S, Wolfgang MJ. 2020. Determining the bioenergetic capacity for fatty acid oxidation in the mammalian nervous system. Mol Cell Biol 40:e00037-20. https://doi.org/10.1128/MCB.00037-20.

Address correspondence to Michael J. Wolfgang, mwolfga1@jhmi.edu.

Received 28 January 2020
Accepted 16 February 2020
Accepted manuscript posted online 2 March 2020
Published 28 April 2020

observed *in vitro* using isolated brain tissue (17, 21–25). Still, the existence, capacity, and relevance of FAO in the brain itself remain highly controversial (26).

The most common perception of brain bioenergetics is that the mammalian brain is metabolically inflexible. While most vertebrate brains that have been studied rely heavily on glucose consumption under normal conditions, there is evidence that some invertebrates consume considerable amounts of fatty acids in nervous tissue beyond early development, which suggests that there may not be an intrinsic disallowance of FAO in the central nervous system (CNS) in other organisms, as well (27). Additionally, in vertebrates, the rate-setting metabolites in FAO (acylcarnitines [ACs]) are dramatically upregulated following many disparate paradigms of nerve injury, suggesting that the mature mammalian nervous system can induce mitochondrial oxidation of FAs, at least under some conditions (28–30). Regardless, a better understanding of FA usage in the mammalian CNS under normal conditions is needed.

Previous studies have described FAO in the brain as improbable. Yang et al. reported that CNS β-oxidation is limited based on brain-isolated mitochondria having 0.7% the relative specific activity of 3-ketoacylthiolase compared to that in heart-isolated mitochondria (26). Clearly, the heart oxidizes more FAs than the CNS, but this is not informative regarding whether FAO is a common metabolic process in the mammalian nervous system. It has been speculated that neurons are unable to safely oxidize long-chain FAs as a major energy substrate due to the high potential for reactive oxygen species (ROS)-mediated damage (31). However, other cell types in the brain (e.g., astrocytes) may utilize long-chain FAs to drive cellular energetics or to dispose of unnecessary or potentially dangerous excess FAs within the nervous system (32).

FAs of all chain lengths are capable of crossing the blood-brain barrier (BBB) (33–35). Long-chain FAs require the carnitine shuttle system for entry into the mitochondrial matrix, while short- and medium-chain FAs can diffuse into the mitochondrial matrix directly for β-oxidation. Carnitine shuttle and β-oxidation genes are expressed primarily in astrocytes and neural stem cells (NSCs) throughout the brain (7, 17, 18). Oxidation of substrates other than glucose is largely believed to occur in preweaning rodents, and the expression of β-oxidative genes and carnitine shuttle genes (*Cpt1a* and *Cpt2*) only continues to increase throughout neurodevelopment in rodents (17, 33).

To understand the bioenergetic capacity for FAO in a mammalian brain, we generated mice with pan-brain-specific loss of the product of an obligate gene in FAO, carnitine palmitoyltransferase 2 ($CPT2^{B-/-}$). We used $CPT2^{B-/-}$ mice to explore the bioenergetic capacity for FAO in the brain and to discern the physiological and behavioral consequences of the loss of FAO in the brain and the contributions of FAO in the CNS to the brain metabolome. Additionally, we compared the brain metabolomes of $CPT2^{B-/-}$ mice and wild-type ($CPT2^{lox/lox}$) mice to those of mice incapable of hepatic FAO ($CPT2^{L-/-}$ mice), which are unable to provide liver-produced ketone bodies to the brain, and peroxisome proliferator-activated receptor α (PPARα) knockout (KO) mice, which display a dysfunctional fasting response. Through biochemical experiments and metabolic phenotyping, behavioral testing, and unbiased and targeted metabolomics, we demonstrate that FAO occurs within the CNS under normal conditions with no impact on FAO metabolites in other tissues, nor is brain FAO influenced by disparate dietary conditions.

RESULTS

Development of mice with a pan-brain-specific loss of fatty acid oxidation. To better understand the bioenergetic capacity for FAO in the mammalian brain and to determine the biochemical and physiological impacts of its loss *in vivo*, we generated mice with a pan-brain-specific KO of CPT2, encoded by an obligate gene for long-chain mitochondrial FAO. Loss of functional CPT2 prevents acyl transfer from carnitine to coenzyme A (CoA), which is necessary for mitochondrial entry, and therefore prevents the subsequent oxidation of long-chain FAs. A mouse model with a *Cpt2* loss-of-function allele was previously generated by flanking exon 4 of the *Cpt2* gene, which contains the protein-coding sequence for catalytically active residues with *loxP* recombination sites ($CPT2^{lox/lox}$) (Fig. 1A) (36). Recombination of exon 4 results in a frameshift

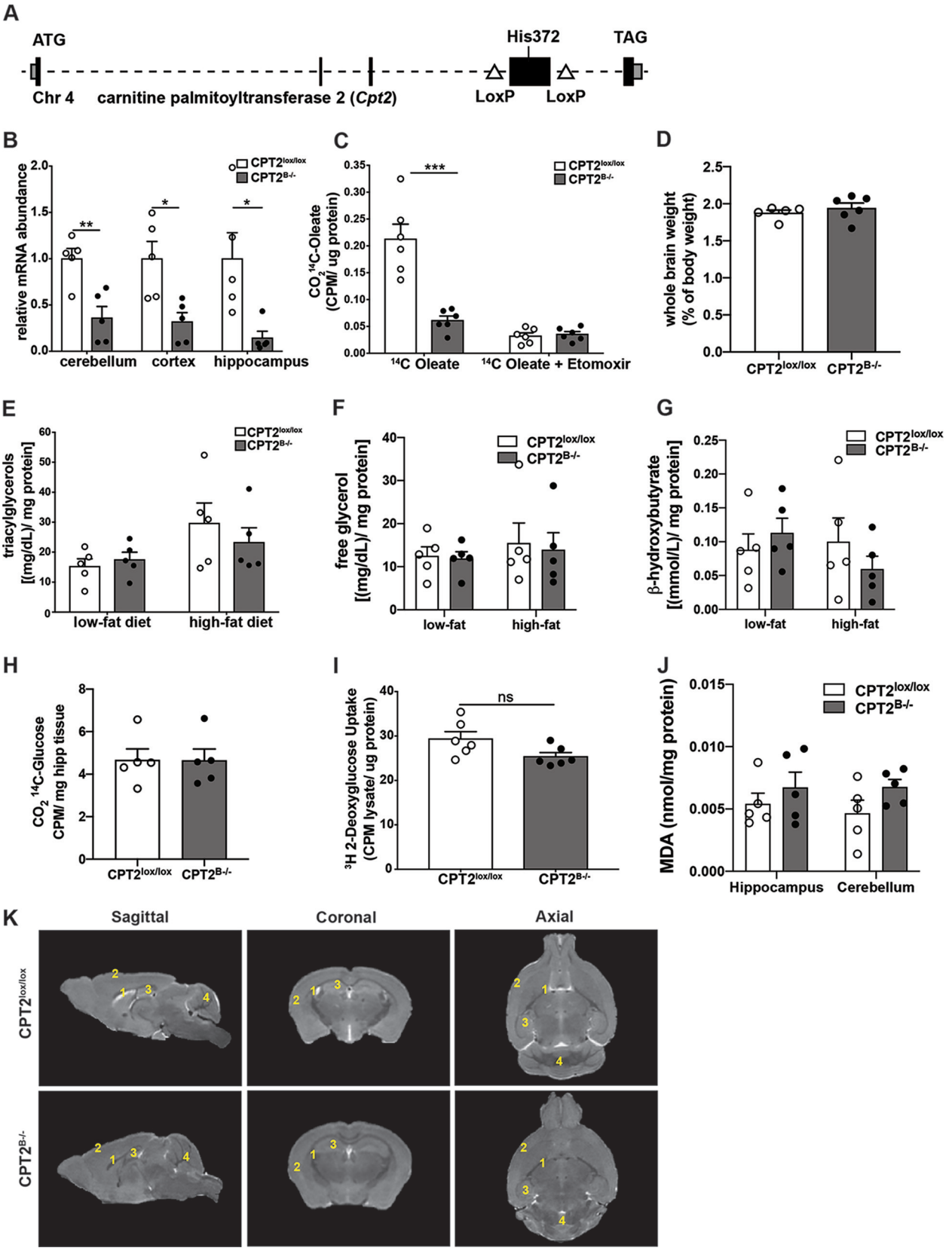

FIG 1 Development of mice with pan-brain-specific deletion of *Cpt2*. (A) Scheme depicting gene-targeting strategy for the *Cpt2* gene. (Adapted from reference 36.) (B) mRNA abundances of *Cpt2* in isolated cerebellum, cortex, and hippocampus from adult $CPT2^{lox/lox}$ and $CPT2^{B-/-}$ mice ($n = 5$). (C) Oxidation of [1-^{14}C]oleic acid to $^{14}CO_2$ in P2 primary cortical astrocytes derived from $CPT2^{lox/lox}$ and $CPT2^{B-/-}$ mice ($n = 6$). [Etomoxir] = 100 μM. CPM, counts per minute. (D) Whole wet weights of $CPT2^{lox/lox}$ ($n = 5$) brains and $CPT2^{B-/-}$ ($n = 6$) brains as a percentage of body weight. (E) Concentrations

(Continued on next page)

of the remaining exons. Generating a mouse line with a pan-brain-specific loss of CPT2 ($CPT2^{B-/-}$) was accomplished by breeding $CPT2^{lox/lox}$ mice with nestin-Cre transgenic mice until they were homozygous for the floxed allele (37). $CPT2^{B-/-}$ mice are viable and fertile. As expected, $CPT2^{B-/-}$ mice exhibited a significant depletion in *Cpt2* mRNA in multiple brain regions, including the cerebellum, cortex, and hippocampus (Fig. 1B).

Astrocytes and NSCs express FA oxidative enzymes at high levels in comparison to neurons and other cell types of the brain (7, 17, 19, 38). Therefore, we generated primary astroglia from $CPT2^{lox/lox}$ (wild-type) and $CPT2^{B-/-}$ mice. Primary postnatal day 2 (P2) cortical astrocytes derived from $CPT2^{B-/-}$ mice resulted in a significant depletion of the ability to fully oxidize [1-^{14}C]oleic acid to $^{14}CO_2$, equivalent to a saturating dose of the FAO inhibitor etomoxir (Fig. 1C) yet with no changes in tissue wet weight in the $CPT2^{B-/-}$ brains (Fig. 1D). Furthermore, brain-specific loss of CPT2 did not lead to an accumulation of triacylglycerol in cortices from $CPT2^{B-/-}$ mice (Fig. 1E), as suggested from studies in invertebrates (39, 40). Changes were also not observed in free glycerol (Fig. 1F) or β-hydroxybutyrate (Fig. 1G). Perhaps less expected, there was no significant compensation in glucose oxidation after loss of FAO in the brain using $CPT2^{B-/-}$ cortex (Fig. 1H) nor compensation in glucose uptake due to loss of *Cpt2* expression in primary P2 cortical astrocytes (Fig. 1I). No significant differences in lipid peroxidation were observed in the hippocampus or cerebellum in $CPT2^{B-/-}$ explants (Fig. 1J). Finally, we generated three-dimensional renderings of whole brains from $CPT2^{B-/-}$ and $CPT2^{lox/lox}$ adult female mice using high-resolution magnetic resonance imaging (MRI) (Fig. 1K). There were no major observable changes in gross brain size or anatomy due to genotype. Regional volumes were calculated using the MRI renderings of $CPT2^{B-/-}$ and $CPT2^{lox/lox}$ brains (see Fig. S1A in the supplemental material). While not significant, lateral ventricles appeared smaller in $CPT2^{B-/-}$ mice. In summary, we generated a model with the loss of a gene necessary for FAO to study the contributions of FAO to CNS bioenergetics, metabolic biochemistry and physiology, and animal behavior.

Brain-specific loss of long-chain fatty acid oxidation does not affect systemic metabolic physiology. It has been suggested that the brain can sense caloric density by linking the central oxidation of FAs to the regulation of body weight and glucose tolerance (41–43). $CPT2^{B-/-}$ mice exhibited a decrease in *Cpt2* mRNA in kidney and gonadal white adipose tissue (gWAT) but did not exhibit changes in the wet weight of any tissue (see Fig. S1C and D). The loss of long-chain FAO in the CNS may result in systemic changes in metabolic biochemistry and/or physiology by disruption of neuroendocrine signaling or, more broadly, by dampening general CNS function and the ability of the brain to communicate with peripheral tissues. Therefore, we examined the parameters of metabolic health in $CPT2^{B-/-}$ mice under low- and high-fat feeding paradigms. Loss of CPT2 in the brain did not result in major body weight changes in 18-week-old $CPT2^{B-/-}$ males or females after a 15-week-long high-fat or low-fat diet (LFD) (Fig. 2A). In $CPT2^{B-/-}$ males, blood glucose was increased 1.5-fold after 15 weeks of LFD, but no significant changes were apparent after an HFD (Fig. 2B) There were also no significant differences in serum lipid metabolites in $CPT2^{B-/-}$ mice at 18 weeks of age after a 15-week-long HFD or LFD (Fig. 2B). These data suggest either brain FAO *per se* is not required for peripheral metabolic health or additional stressors may be necessary to uncover whether long-chain FAO in the CNS has a role in the maintenance of systemic metabolic homeostasis *in vivo*.

Loss of brain-specific long-chain fatty acid oxidation has a subtle impact on behavior. While the functional role(s) of long-chain FAO within the mammalian brain

FIG 1 Legend (Continued)
of triacylglycerol in cortical tissue in 18-week-old $CPT2^{lox/lox}$ and $CPT2^{B-/-}$ mice after 15 weeks of low-fat or high-fat diet ($n = 5$). (F) Concentrations of free glycerol in cortical tissue in 18-week-old $CPT2^{lox/lox}$ and $CPT2^{B-/-}$ mice after 15 weeks of low-fat or high-fat diet ($n = 5$). (G) Concentrations of β-hydroxybutyrate in cortical tissue in 18-week-old $CPT2^{lox/lox}$ and $CPT2^{B-/-}$ mice after 15 weeks of low-fat or high-fat diet ($n = 5$). (H) Oxidation of [U-^{14}C]glucose to $^{14}CO_2$ using approximately 30 mg of *ex vivo* brain tissue from $CPT2^{lox/lox}$ and $CPT2^{B-/-}$ mice ($n = 5$). (I) Uptake of [^{3}H]2-deoxyglucose into P2 primary cortical astrocytes derived from $CPT2^{lox/lox}$ and $CPT2^{B-/-}$ mice ($n = 6$). (J) A TBARS assay used hippocampus and cerebellum tissues from $CPT2^{lox/lox}$ and $CPT2^{B-/-}$ mice ($n = 5$). (K) Representative MRI renderings of sagittal, axial, and coronal planes from $CPT2^{lox/lox}$ and $CPT2^{B-/-}$ mice. 1, lateral ventricles; 2, cortex; 3, hippocampus; 4, cerebellum. The data are expressed as means and standard errors of the mean (SEM). The data shown were analyzed using Student two-tailed *t* tests. *, $\alpha = 0.05$; **, $\alpha = 0.01$; ***, $\alpha = 0.001$; ns, not significant.

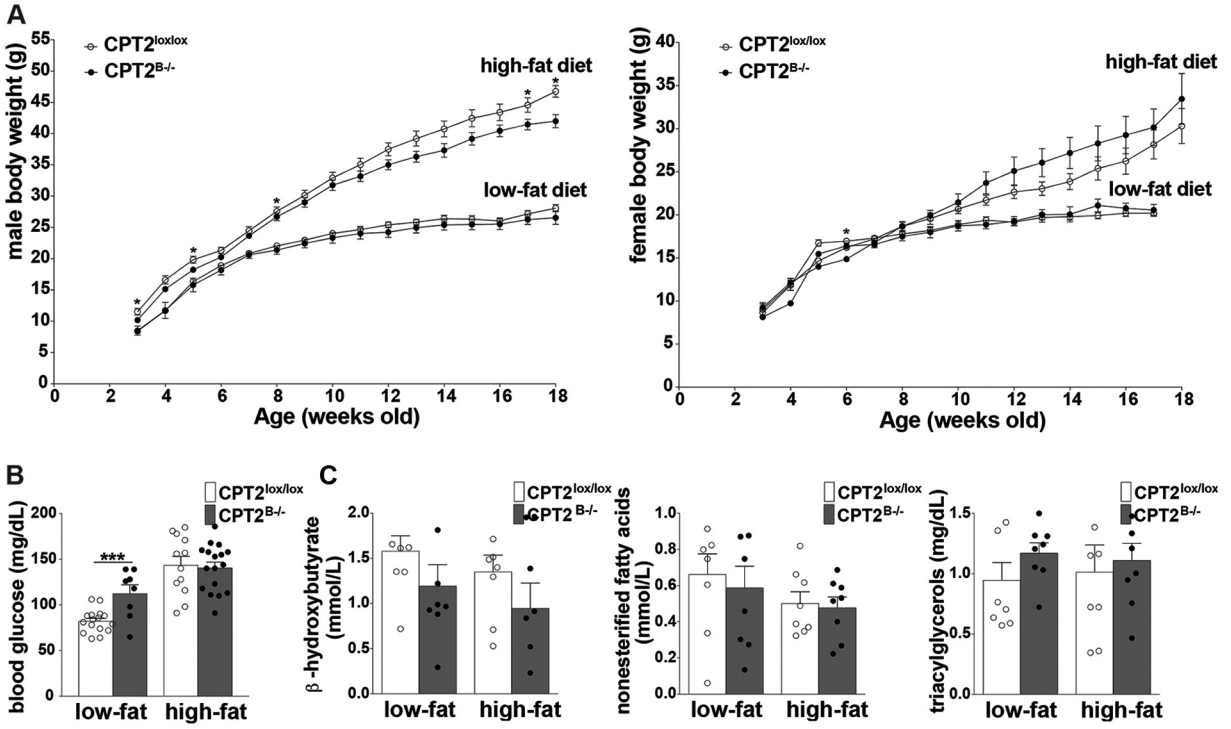

FIG 2 Brain-specific loss of long-chain fatty acid oxidation does not systemically affect peripheral metabolism in CPT2$^{B-/-}$ mice. (A) Body weights of male and female CPT2$^{lox/lox}$ and CPT2$^{B-/-}$ mice from the beginning of low-fat or high-fat diets at 3 weeks of age to 18 weeks of age. Males, CPT2$^{lox/lox}$, low-fat, $n = 16$, and high-fat, $n = 14$; CPT2$^{B-/-}$, low-fat, $n = 8$, and high-fat, $n = 17$. Females, CPT2$^{lox/lox}$, low-fat, $n = 9$, and high-fat, $n = 14$; CPT2$^{B-/-}$, low-fat, $n = 3$, and high-fat, $n = 13$. The data were analyzed using Student two-tailed *t* tests. (B) Blood glucose in 18-week-old male CPT2$^{lox/lox}$ and CPT2$^{B-/-}$ mice after 15 weeks of low-fat and high-fat diets. CPT2$^{lox/lox}$, low fat, $n = 16$, and high fat, $n = 14$; CPT2$^{B-/-}$, low fat, $n = 8$, and high fat, $n = 17$. (C) Serum metabolites (β-hydroxybutyrate, NEFAs, and triacylglycerol) in 18-week-old male CPT2$^{lox/lox}$ and CPT2$^{B-/-}$ mice after 15 weeks of low-fat and high-fat diets. CPT2$^{lox/lox}$, low fat, $n = 8$, and high fat, $n = 8$; CPT2$^{B-/-}$, low fat, $n = 8$, and high fat, $n = 8$. The data were analyzed using ordinary two-way analysis of variance with Sidak's test for multiple comparisons. The data are expressed as means ± SEM. *, $\alpha = 0.05$; ***, $\alpha = 0.001$.

is unknown, it is known that total lipid abundance in the brain is high and that the brain lipid composition is specialized to maintain proper structure and function (15, 16). Inborn errors in FAO have been associated with neurodevelopmental abnormalities (4–7). The previous reports are based on total systemic loss of mitochondrial β-oxidation. However, the specific impact of FAO loss in the brain on animal behavior is not known. Perhaps behavioral defects can be attributed to neurodevelopmental delays due to perturbations in NSC homeostasis after loss of FAO (7). To determine the behavioral impact due to the loss of FAO in the brains of mice, we performed behavioral tests to learn about emotionality, motor function, and social memory recall.

To determine the effects of FAO loss in the brain on mouse ambulation and emotionality, we conducted a 3-zone open-field test using adult CPT2$^{B-/-}$ and CPT2$^{lox/lox}$ mice (Fig. 3A). Nestin-Cre expression has no known impact on ambulation using open-field testing (44), nor did we find any changes in ambulation and emotionality attributed to the nestin-Cre transgene after repeating the 3-zone open-field tests described below using mice heterozygous for the floxed *Cpt2* allele (CPT2$^{lox/+}$) with or without the nestin-Cre transgene allele (see Fig. S2 in the supplemental material). For 3-zone open-field testing, mice were allowed to roam freely within the testing apparatus for 5 min. The total movement pattern was traced using AnyMaze software (Stoelting Co., Wood Dale, IL), which recorded ambulatory parameters, such as zone entry number, average velocities, distances traveled, time spent in zones, and number of immobile episodes (Fig. 3B to D; see Fig. S3 in the supplemental material) (12, 45). Additional behaviors indicative of emotionality, such as hind-leg rearing episodes and grooming episodes, were also recorded during the testing time (Fig. 3D). Typically, rodents display an aversion to wide-open, well-lit spaces and tend to move along the

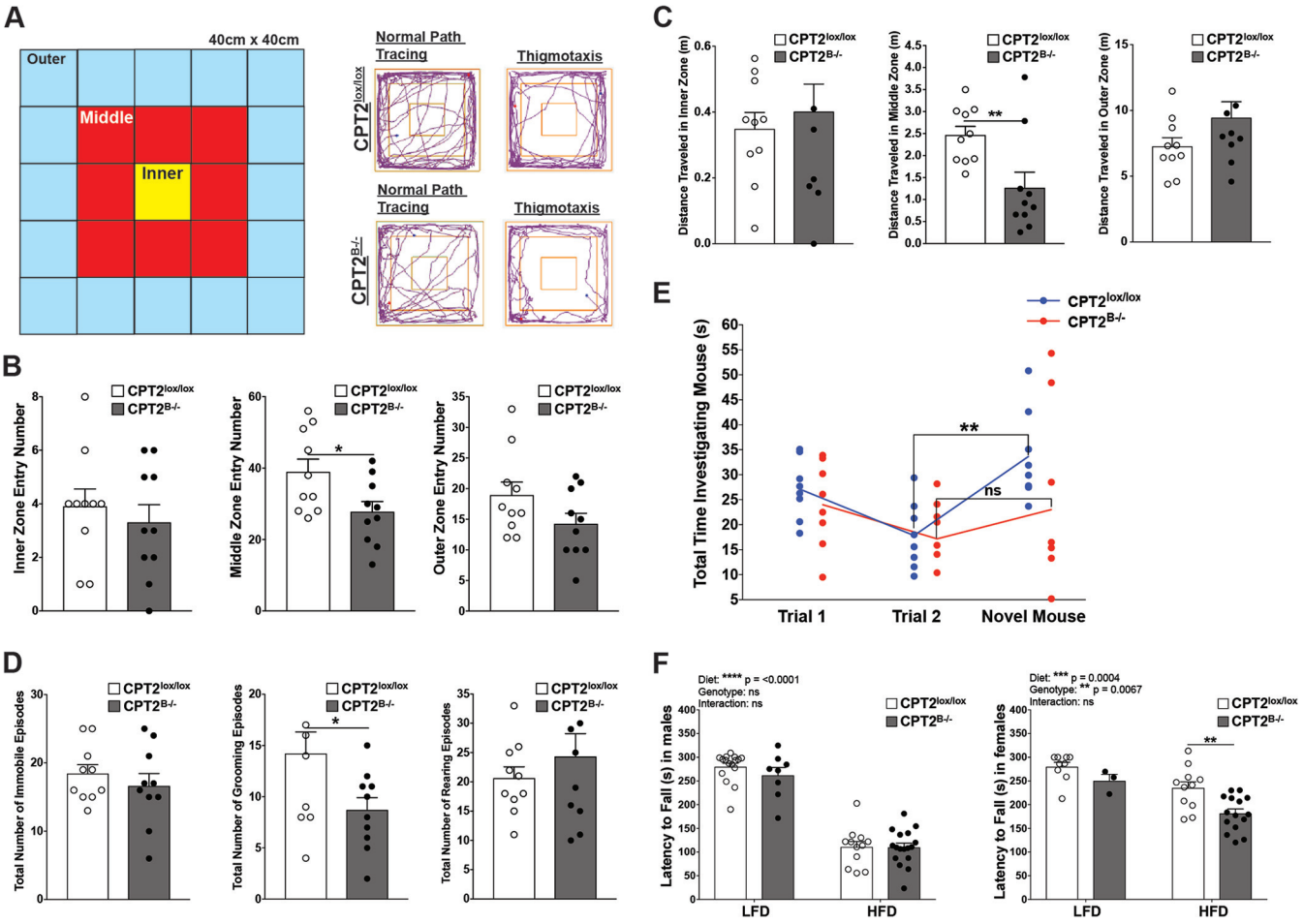

FIG 3 Loss of brain-specific long-chain fatty acid oxidation results in a subtle impact on animal behavior. (A to D) Three-zone open-field test. (A) Key for operationalization of inner, middle, and outer zones in 3-zone open-field test. Shown are representative path traces from adult female $CPT2^{lox/lox}$ and $CPT2^{B-/-}$ mice depicting normal movement and thigmotaxis. (B) Total number of times the inner, middle, and outer zones were entered by adult female $CPT2^{lox/lox}$ and $CPT2^{B-/-}$ mice ($n = 10$). Shown are total percentages of time spent in the inner, middle, and outer zones by adult female $CPT2^{lox/lox}$ and $CPT2^{B-/-}$ mice ($n = 10$). The data were analyzed using Student two-tailed *t* tests. (C) Total distances traveled in inner, middle, and outer zones by adult female $CPT2^{lox/lox}$ and $CPT2^{B-/-}$ mice ($n = 10$). The data were analyzed using Student two-tailed *t* tests. (D) Total numbers of immobile episodes, grooming episodes, and rearing episodes in adult female $CPT2^{lox/lox}$ and $CPT2^{B-/-}$ mice ($n = 10$). The data were analyzed using Student two-tailed *t* tests. (E) Three-trial social recognition test. Shown are the total amounts of time adult female $CPT2^{lox/lox}$ and $CPT2^{B-/-}$ mice spent investigating a pup initially (Trial 1; $n = 8$) and in a subsequent investigation (Trial 2; $n = 8$) and time spent investigating a novel pup after the first two trials (Novel Mouse; $n = 8$). The data were analyzed using repeated-measures two-way analysis of variance with Sidak tests for multiple comparisons. (F) Rotarod test. Shown is latency to fall in rotarod tests performed on adult male and female $CPT2^{lox/lox}$ and $CPT2^{B-/-}$ mice on LFD and HFD. Males, $CPT2^{lox/lox}$, low fat ($n = 16$) and high fat ($n = 12$); $CPT2^{B-/-}$, low fat ($n = 8$) and high fat ($n = 17$). Females, $CPT2^{lox/lox}$, low fat ($n = 9$) and high fat ($n = 11$); $CPT2^{B-/-}$, low fat ($n = 3$) and high fat ($n = 15$). The data were analyzed using ordinary two-way analysis of variance with Sidak tests for multiple comparisons. The data are expressed as means and SEM. *, $\alpha = 0.05$; **, $\alpha = 0.01$; ns, not significant.

periphery of an open environment. Mice in the presence of stressors, such as a predators, dietary fasting, or pharmacological-induced anxiety, all display heightened, stereotyped movement along a solid wall, also known as thigmotaxis (46). Therefore, increased thigmotaxis is used as a measure of increased anxiety in mice. Mice in the 3-zone open-field test displayed thigmotaxis via stereotyped movement by circling the outer zone (Fig. 3A). There was no significant difference in the total percentages of the 5-min testing period spent in the inner, middle, or outer zone between $CPT2^{B-/-}$ and $CPT2^{lox/lox}$ mice. The total numbers of times a mouse entered the innermost and outermost zones were not significantly different between $CPT2^{B-/-}$ and $CPT2^{lox/lox}$ mice. However, the total number of entries into the middle zone was significantly decreased in $CPT2^{B-/-}$ mice in comparison to $CPT2^{lox/lox}$ mice (Fig. 3B; see Fig. S3A). In each zone, the average velocity at which the mice traveled was not significantly changed due to genotype, yet the total distance traveled for $CPT2^{B-/-}$ mice compared to $CPT2^{lox/lox}$ mice in the middle zone was significantly down (Fig. 3C; see Fig. S3B). The

ability of CPT2$^{B-/-}$ mice to maintain the same speed as CPT2$^{lox/lox}$ mice is likely indicative of the retention of normal motor function. While we did observe some significant changes in zone entry numbers and grooming behaviors, these data alone are not sufficient to support a strong behavioral impairment due to loss of CPT2.

Other behavioral measures of anxiety in the open-field test, such as the number of immobile episodes and the total number of rearing episodes, were not significantly different between CPT2$^{B-/-}$ and CPT2$^{lox/lox}$ mice (Fig. 3D). Grooming is a complex behavior in mice, with a stereotyped pattern of movement and duration of activity. Irregularities in the pattern or decreases in the duration of grooming activity have been used as an indicator of panic and anxiety in rodents (47). In CPT2$^{B-/-}$ mice, we observed a decrease in grooming episodes compared to CPT2$^{lox/lox}$ mice (Fig. 3D). Nestin-Cre-expressing mice have been reported by others to have a depressed fear response, which is contradictory to our observed decrease in grooming episodes (44).

Errors in FAO in humans have been associated with neurodevelopmental abnormalities common to ASDs, including speech delay and social impairment (4–7). Loss of CNS FAO may also affect social memory and cognitive capabilities in CPT2$^{B-/-}$ mice. Three-trial social memory tests using CPT2$^{B-/-}$ and CPT2$^{lox/lox}$ dams as subject mice and pups as the intruder test mice were conducted to test for social memory deficits (5, 48). For two 5-min trials, our subject dams were paired with the same intruder pup within a testing cage. In mice with normal cognition and social memory, subject mouse interest in the intruder pup decreases with subsequent exposures. This habituation was quantified between trials by recording the total time the subject mouse investigated the intruder over the total 5 min. A novel intruder pup was paired with the subject mouse during the third (final) trial. A subject mouse with normal cognition and memory would normally investigate the novel pup for a longer time than the investigation times in repeated exposures to the previous pup, which demonstrates dishabituation (5, 48). Both CPT2$^{B-/-}$ and CPT2$^{lox/lox}$ dams displayed the paradigm decrease in time spent investigating a familiar pup when the sequential trials 1 and 2 were compared (Fig. 3E). Upon introduction of a novel pup in the testing cage, only CPT2$^{lox/lox}$ dams demonstrated a significant increase in total time spent investigating the novel pup, which supports dishabituation of their previous conditioning (Fig. 3E). CPT2$^{B-/-}$ dams failed to demonstrate recovery from previous conditioning in the presence of a novel stimulus. However, in summary, these data, while significant, do not represent a robust impaired behavioral phenotype.

As an additional measure of motor coordination and to determine the impact of diet on motor coordination, 12-week-old CPT2$^{B-/-}$ and CPT2$^{lox/lox}$ mice were subjected to a rotarod test while on a low- or high-fat feeding paradigm. Regardless of genotype, males and females on an HFD exhibited decreased time on the rotarod compared to LFD mice, which indicates impaired motor coordination under dietary stress (Fig. 3F). In males, there was no difference in latency to fall from the rotarod between CPT2$^{B-/-}$ mice and CPT2$^{lox/lox}$ mice on either an LFD or an HFD. In females, there was no significant difference in latency to fall between CPT2$^{B-/-}$ and CPT2$^{lox/lox}$ mice on an LFD. However, there was a significant decrease in latency to fall in CPT2$^{B-/-}$ females on an HFD compared to CPT2$^{lox/lox}$ females fed an HFD (Fig. 3F). While CPT2$^{B-/-}$ mice exhibited mild motor impairments in disparate dietary states, such as an HFD, motor function was largely unaltered by loss of functional CPT2 in the brain.

Deletion of *Cpt2* in the nervous system results in elevated expression of β-oxidation enzymes. To understand the impact of *Cpt2* deletion on molecular mechanisms in the CNS, we measured the transcription of genes related to FAO, indicative of CNS inflammation and stress, and related to BBB integrity in cortices from CPT2$^{B-/-}$ and CPT2$^{lox/lox}$ mice that were either fed a normal chow diet (fed) or subjected to a 24-h fast (fasted) and in a separate cohort of mice subjected to 15 weeks of an HFD or an LFD. No significant changes in transcription were observed in CNS stress markers, BBB integrity, or autophagy genes between CPT2$^{B-/-}$ and CPT2$^{lox/lox}$ cortices across any dietary conditions (Fig. 4A, C, D, and E). Carnitine palmitoyltransferase 1a (*Cpt1a*) and acyl-CoA dehydrogenase (*Acadl*) mRNAs were significantly elevated in both

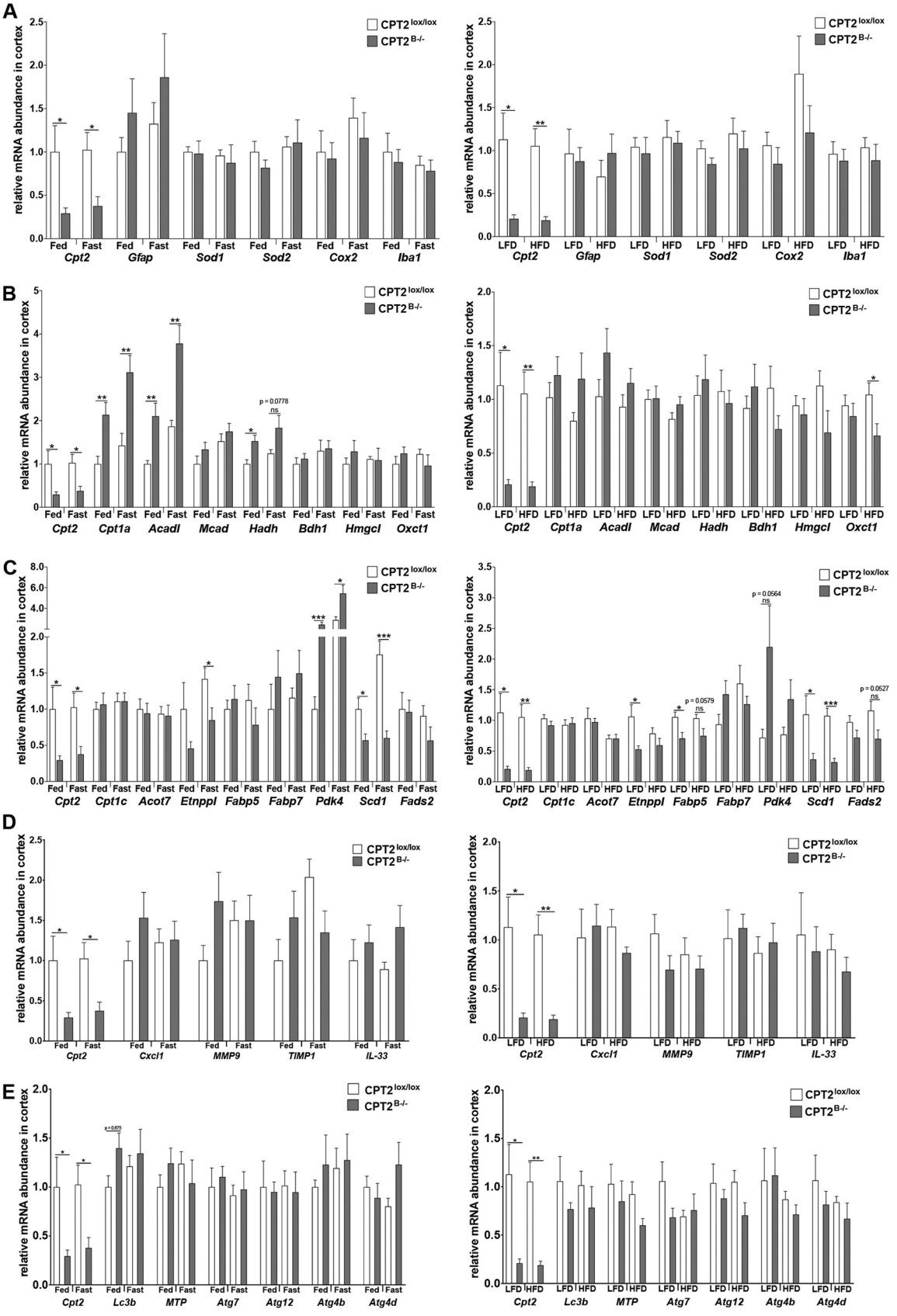

FIG 4 Contributions of brain-specific fatty acid oxidation to CNS structure and function. Shown is mRNA abundance in cortices from male 9-week-old fed and 24-h-fasted CPT2$^{lox/lox}$ and CPT2$^{B-/-}$ mice ($n = 6$) and mRNA abundance in cortices from 18-week-old CPT2$^{lox/lox}$ and

(Continued on next page)

fed and fasted CPT2$^{B-/-}$ cortices compared to CPT2$^{lox/lox}$ cortex (Fig. 4B). Hydroxyacyl-CoA dehydrogenase (*Hadh*) mRNA was significantly elevated in cortices from CPT2$^{B-/-}$ mice only under fed conditions (Fig. 4B). These data are consistent with the transcriptional response of the liver to a loss of FAO (49, 50) and suggest PPARα-dependent regulation within the CNS (51).

Long-chain acylcarnitines accumulate in the hippocampus in CPT2$^{B-/-}$ mice. If the mammalian brain oxidizes long-chain FAs substantially, then loss of FAO would be predicted to result in dramatic changes in the metabolic profile of the brain. While the contributions of FAO in the brain are not well defined, during fasting, the brain has been shown to switch from using mainly glucose to the utilization of a significant proportion of ketone bodies derived from hepatic FAO (49). To explore the impact of panbrain *Cpt2* deletion on the relative metabolite profile in the brain, we used 24-h-fasted 9-week-old male mouse hippocampi (a highly metabolically active region of the brain) from several unique models of impaired lipid catabolism to address outstanding questions in neurometabolism (Fig. 5A). Hippocampi from CPT2$^{B-/-}$ mice were used to investigate the influence of FAO in the CNS on the brain metabolome. Hippocampi from mice with a liver-specific deletion of *Cpt2* (CPT2$^{L-/-}$) were used to investigate the influence of hepatic FAO and ketone body delivery on CNS metabolism. CPT2$^{lox/lox}$ hippocampi were used as the wild-type control, and hippocampi from PPARα KO (PPAR$\alpha^{-/-}$) mice were used to address changes in the metabolic profile in the CNS that are attributed to the loss of the major transcriptional mediator of the fasting response (Fig. 5A). Utilizing global unbiased metabolomics, we determined the relative abundances of 568 metabolites. The relative differences in abundance between metabolites across genotypes were summarized in a principal-component analysis (PCA). The PCA of the relative metabolite summary indicates that the relative abundances of metabolites from these genotypes were nicely separated, with PPAR$\alpha^{-/-}$ hippocampus being the most dissimilar (Fig. 5B). Importantly, this demonstrates that a loss of PPARα is not synonymous with a loss in β-oxidation, as is often suggested. These data show that the CNS metabolome is uniquely affected by tissue-specific deficits in FA catabolism.

CPT2$^{B-/-}$ mice are incapable of transferring an acyl chain from carnitine to coenzyme A for activation in the mitochondrial matrix for β-oxidation. While intermediates in major metabolic pathways, including the tricarboxylic acid (TCA) cycle and glycolysis, were largely unchanged (see Fig. S4 in the supplemental material), long-chain ACs exhibited a stark elevation in fasted CPT2$^{B-/-}$ hippocampus—between 8- and 38-fold, depending on the molecular species—compared to fasted CPT2$^{lox/lox}$ hippocampus or any other genotype (Fig. 5C). We observed that CPT2 loss in primary P2 cortical astrocytes led to an inability to oxidize [1-^{14}C]oleic acid to $^{14}CO_2$ (Fig. 1C). When *Cpt2* is deleted in the brain, the inability to transport local acyl chains via the carnitine shuttle in mitochondria results in a deficient capacity for oxidation of long-chain FAs and an accumulation of long-chain AC species (Fig. 5C). These data provide strong evidence that mitochondrial long-chain FAO (whether using local FAs or FAs transported from peripheral tissues) occurs at a high level in the brain under normal conditions.

Oxidation of fatty acids in the liver is required to sustain ketone bodies in the CNS upon fasting. Ketone bodies are primarily generated by long-chain FAs in the liver (49). However, others have reported that astrocytes can use FAO to generate ketone bodies to fuel neuron function locally (20, 21, 52). Perhaps long-chain FAO in the CNS is necessary to regulate concentrations of ketone bodies used by the brain upon fasting. In the relative metabolite summary described above, the ketone body β-hydroxybutyrate was significantly depleted (4.65-fold) in hippocampi from fasted

FIG 4 Legend (Continued)
CPT2$^{B-/-}$ mice after 15 weeks on a low-fat or high-fat diet ($n = 6$). Expression of the following genes was evaluated: genes related to CNS health and inflammation (A), genes related to oxidative metabolism (B), metabolic genes with major expression in the CNS (C), BBB integrity genes (D), and autophagy genes (E). The data are expressed as means and SEM. The data were analyzed using Student two-tailed *t* tests. *, $\alpha = 0.05$; **, $\alpha = 0.01$; ***, $\alpha = 0.001$; ns, not significant.

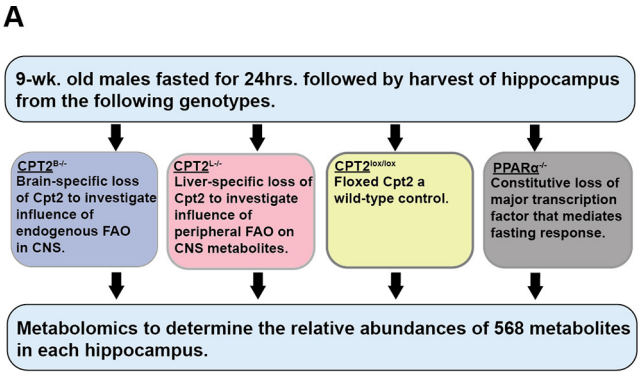

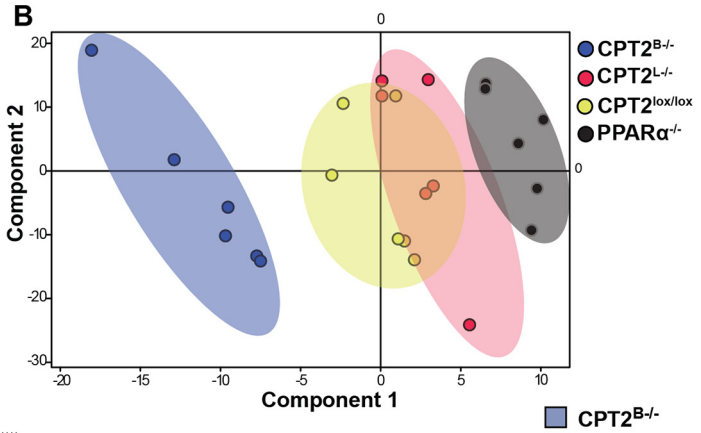

C

Long-chain Acylcarnitines (Fold Change to CPT2$^{lox/lox}$)

chain length	CPT2$^{B-/-}$	CPT2$^{L-/-}$	PPARα$^{-/-}$
C18:3	37.869	1.372	2.589
C16:1	17.834	0.973	1.116
C18:0	10.330	0.894	0.856
C18:1	9.310	0.870	0.837
C18:2	9.120	1.124	1.469
C14:1	9.118	0.955	3.323
C16:0	7.651	0.827	0.969

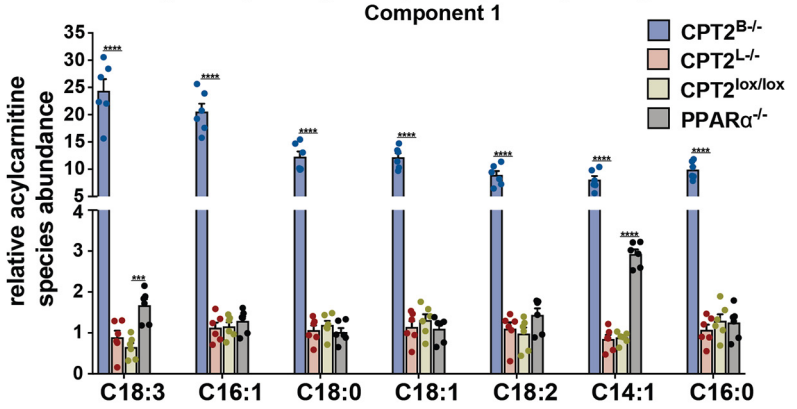

D

C4 Species (Fold Change to CPT2$^{lox/lox}$)

Species	CPT2$^{B-/-}$	CPT2$^{L-/-}$	PPARα$^{-/-}$
carnitine	1.174	0.596	0.867
3-hydroxybutyrate	1.508	0.214	0.521
3-hydroxybutyrylcarnitine (1)	0.456	0.141	0.553

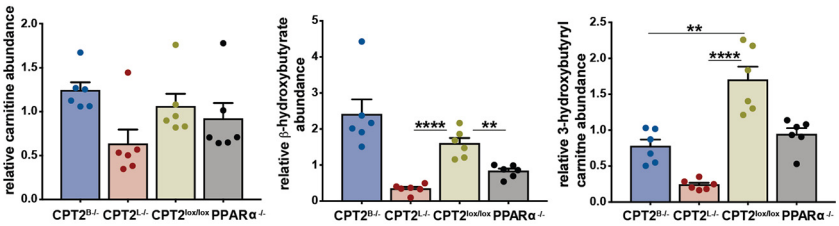

E

Co-factors (Fold Change to CPT2$^{lox/lox}$)

Species	CPT2$^{B-/-}$	CPT2$^{L-/-}$	PPARα$^{-/-}$
coenzyme A	1.999	1.323	1.882
phosphopantetheine	1.837	1.062	1.676
3'-dephosphocoenzyme A	2.040	1.096	1.338
pantothenate	0.938	0.753	0.374

Short-chain Acylcarnitines (Fold Change to CPT2$^{lox/lox}$)

chain length	CPT2$^{B-/-}$	CPT2$^{L-/-}$	PPARα$^{-/-}$
isobutyrylcarnitine (C4:0)	0.496	0.552	0.820
3-hydroxybutyrylcarnitine (1)	0.456	0.141	0.553
isovalerylcarnitine (C5:0)	0.394	0.421	0.882
2-methylbutyrylcarnitine (C5:0)	0.386	0.397	0.679
malonylcarnitine	0.335	0.508	0.675
3-hydroxybutyrylcarnitine (2)	0.293	0.343	0.768
adrenoylcarnitine (C22:4)	0.169	0.193	0.191
butyrylcarnitine	0.168	0.271	0.996
glutarylcarnitine (C5:0-DC)	0.098	0.200	1.702

Amino Acids (Fold Change to CPT2$^{lox/lox}$)

Species	CPT2$^{B-/-}$	CPT2$^{L-/-}$	PPARα$^{-/-}$
2-hydroxybutyrate	1.500	0.286	0.864
3-hydroxyisobutyrate	1.479	0.975	0.995
carboxyethyl-GABA	0.632	0.898	0.997
N-acetylarginine	0.397	0.991	0.335
N-acetylasparagine	0.629	1.278	0.814
N-acetylglutamine	0.508	2.333	0.776
N-acetylglycine	1.331	0.297	0.693
N-acetylleucine	0.640	1.129	1.151
N-acetyltyrosine	0.566	3.323	1.665
ophthalmate	1.565	0.240	0.906
N-acetylphenylalanine	0.497	2.742	1.673
N-acetylaspartate	0.950	1.054	0.954

Sphingolipids (Fold Change to CPT2$^{lox/lox}$)

Species	CPT2$^{B-/-}$	CPT2$^{L-/-}$	PPARα$^{-/-}$
glycosyl-N-(2-hydroxynervonoyl)-sphingosine	0.535	0.734	0.673
glycosyl-N-nervonoyl-sphingosine	0.625	0.778	0.958
sphingomyelin	3.446	1.185	1.198

Phospholipids (Fold Change to CPT2$^{lox/lox}$)

Species	CPT2$^{B-/-}$	CPT2$^{L-/-}$	PPARα$^{-/-}$
1,2-dilinoleoyl-GPC	2.005	1.513	2.812
1-linoleoyl-2-arachidonoyl-GPC	1.530	1.322	1.850
1-myristoyl-2-arachidonoyl-GPC	3.332	1.261	1.372
1-oleoyl-2-linoleoyl-GPC	1.402	1.213	1.770
1-palmitoleoyl-2-linoleoyl-GPC	3.789	1.632	2.181
1-palmitoyl-2-gamma-linolenoyl-GPC	5.828	1.466	1.881
1-palmitoyl-2-linoleoyl-GPC	1.496	1.126	1.389
1,2-dilinoleoyl-GPE	2.823	1.907	2.902
1-oleoyl-2-linoleoyl-GPE	1.606	1.198	1.413
1-(1-enyl-palmitoyl)-2-linoleoyl-GPE	1.552	0.959	1.198

PUFAs (Fold Change to CPT2$^{lox/lox}$)

Species	CPT2$^{B-/-}$	CPT2$^{L-/-}$	PPARα$^{-/-}$
docosapentaenoate	0.053	0.440	0.870
hexadecadienoate	58.925	1.946	8.797
linoleate	20.893	1.292	4.806
stearidonate	176.459	2.258	17.999

FIG 5 Loss of CPT2 in the brain results in elevated long-chain acylcarnitines in relative metabolite summary. (A) Flowchart describing unbiased mass spectrometry metabolomics in hippocampi from 9-week-old male 24-h-fasted mice across genotypes. (B) PCA summarizing similarities and dissimilarities of metabolites across genotypes of the relative metabolite summary. (C) Fold changes and relative abundances of long-chain acylcarnitines in whole hippocampi from 24-h-fasted 9-week-old CPT2$^{B-/-}$, CPT2$^{L-/-}$, and PPARα$^{-/-}$ mice in comparison and normalized to CPT2$^{lox/lox}$ mice ($n = 6$). (D) Fold changes and relative abundances of fatty acid-associated metabolites in whole hippocampi from 24-h-fasted 9-week-old CPT2$^{B-/-}$, CPT2$^{L-/-}$, and PPARα$^{-/-}$ mice in comparison and

(Continued on next page)

mice with hepatic loss of CPT2 ($CPT2^{L-/-}$) compared to hippocampi from fasted $CPT2^{lox/lox}$ mice. There was no significant difference in the relative abundance of β-hydroxybutyrate in hippocampi from fasted mice when *Cpt2* was specifically deleted in the brain ($CPT2^{B-/-}$) (Fig. 5D). These data suggest that if *de novo* ketogenesis is occurring in the CNS, it is not sufficient to meet the demands for ketone bodies in the brain following an acute 24-h fast. Surprisingly, the loss of ketone bodies, a major fuel for neurons during a fast, did not result in an energy crisis in the CNS.

Unexpected contribution of fatty acid oxidation to the brain metabolome. Long-chain ACs in the brain reportedly have roles outside of β-oxidation, including stabilizing membrane composition and modulating gene transcription (53, 54). In our metabolite summary described above, we observed a number of enriched metabolites in $CPT2^{B-/-}$ hippocampus that may be increased due to stark elevations in specific ACs (Fig. 5). Molecular species of long-chain ACs, including palmitoyl-L-carnitine, are incorporated into lipids, such as sphingomyelin, phosphatidylcholine, and phosphatidylserine, when NB-2a neuroblastoma cells are supplemented with them (55). The relative abundance of sphingomyelin was elevated 3.45-fold in $CPT2^{B-/-}$ hippocampus compared to $CPT2^{lox/lox}$ hippocampus, likely due to higher availability of palmitoyl-L-carnitine (Fig. 5E). Increased phospholipids in $CPT2^{B-/-}$ hippocampus may also be the result of elevated concentrations of long-chain AC species available for incorporation into phospholipid (Fig. 5E). These data are consistent with an increased incorporation of lipids in the absence of FAO.

Interestingly, several metabolites of the coenzyme A-biosynthetic pathway were elevated in hippocampi of fasted $CPT2^{B-/-}$ mice compared to those of $CPT2^{lox/lox}$ mice, including a 2-fold increase in CoA and the CoA biosynthesis intermediates phosphopantetheine and 3′ dephosphocoenzyme A (Fig. 5E). Palmitoyl-L-carnitine has been shown to potently disinhibit pantothenate kinase 2 (PanK2), which is required for the biosynthesis of coenzyme A (56). Elevated CoA intermediates were likely attributable to increased palmitoyl-L-carnitine (a 7.65-fold increase in $CPT2^{B-/-}$ hippocampus) or similar-chain-length AC species disinhibiting PanK2 in the CNS. These data represent a clear physiological validation of this regulation.

Other classes of metabolites were affected by the loss of long-chain FAO by unknown means, including drastic changes in individual polyunsaturated fatty acids (PUFAs), decreased short-chain ACs, and decreased *N*-acetyl amino acids (Fig. 5E). Short-chain ACs may be consumed when long-chain ACs are unavailable for oxidation in the CNS. Acetyl groups resulting from the oxidation of long-chain ACs may be required for incorporation into *N*-acetyl amino acids.

Fatty acid oxidation within the brain is not impacted by diet and has no impact on systemic acylcarnitines. In order to quantitatively measure if FAO in the brain is modulated based on diet, we measured steady-state concentrations of AC species by targeted metabolomics in cortices from male $CPT2^{lox/lox}$ and $CPT2^{B-/-}$ mice. Cortices from fed and 24-h-fasted mice were collected at 9 weeks of age. Also, cortex tissues were collected from 18-week-old male $CPT2^{lox/lox}$ and $CPT2^{B-/-}$ mice after a 15-week-long low- or high-fat diet. The steady-state concentrations of total ACs were determined by taking the sum of all ACs with the exception of free carnitine. Steady-state concentrations of total ACs in $CPT2^{B-/-}$ cortex were elevated compared to $CPT2^{lox/lox}$ cortex within a range of approximately 1.5- to 2.5-fold across all dietary states (Fig. 6A and B). Acetylcarnitine was modestly, but significantly, decreased in fed $CPT2^{B-/-}$ cortex compared to $CPT2^{lox/lox}$ cortex, but steady-state concentrations of acetylcarni-

FIG 5 Legend (Continued)
normalized to $CPT2^{lox/lox}$ mice ($n = 6$). (E) Fold changes and relative abundances of additional metabolites in whole hippocampi from 24-h-fasted 9-week-old $CPT2^{B-/-}$, $CPT2^{L-/-}$, and $PPAR\alpha^{-/-}$ mice in comparison and normalized to $CPT2^{lox/lox}$ mice ($n = 6$). (C to E) (Left) The data are represented as fold changes in $CPT2^{B-/-}$, $CPT2^{L-/-}$, and $PPAR\alpha^{-/-}$ mice in comparison to $CPT2^{lox/lox}$ mice. The statistical significance of the metabolites shown was determined using the two-stage false-discovery rate (FDR) method of Benjamini, Krieger, and Yekutieli with an FDR (*Q*) of 10%. Fold changes in green boxes are significantly increased, fold changes in red boxes are significantly decreased, and fold changes in yellow boxes are not significantly affected by genotype. (Right) The same data are represented as means of relative species abundance plus SEM in the graphs. **, $\alpha = 0.01$; ****, $\alpha = 0.0001$.

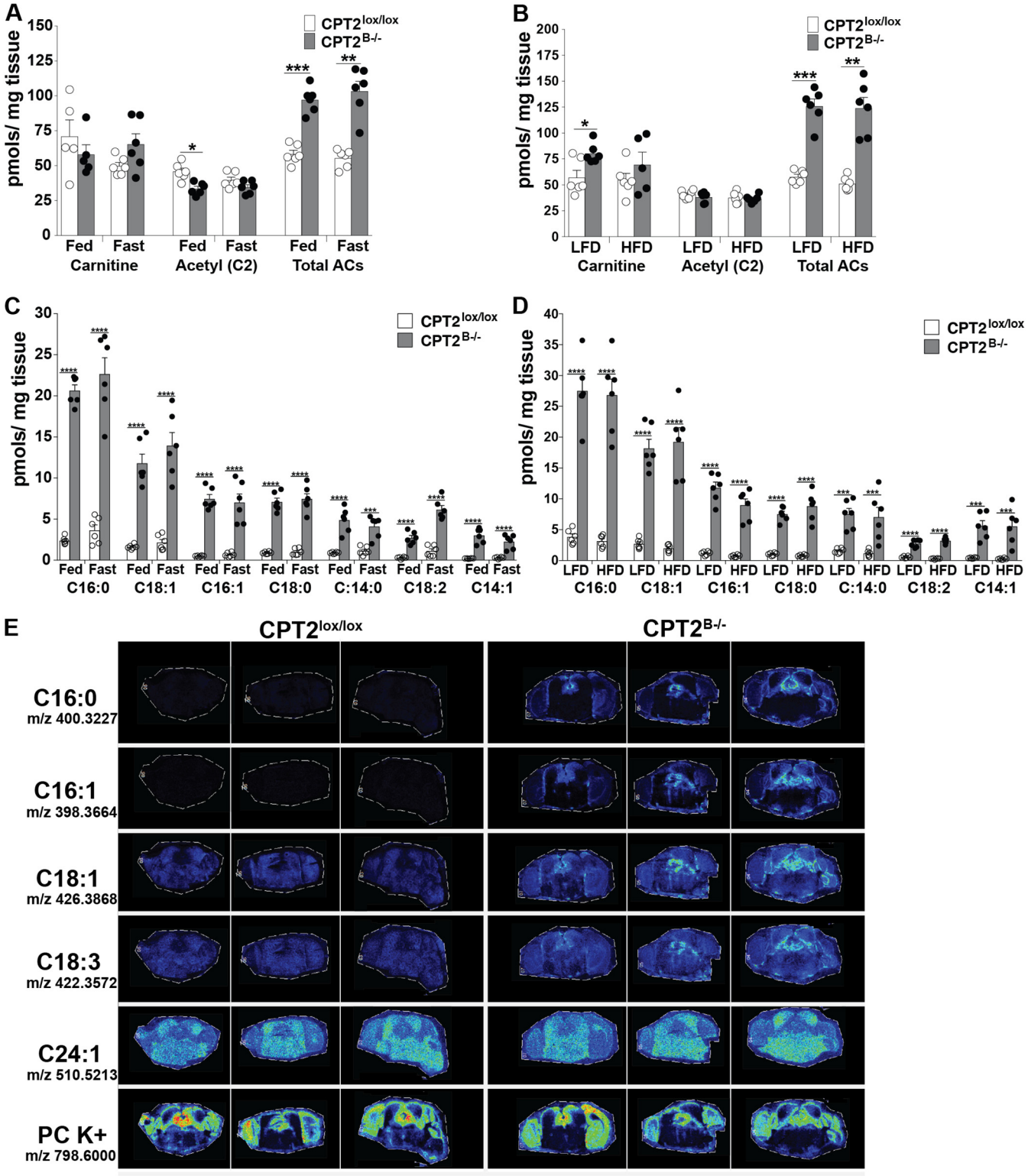

FIG 6 Long-chain acylcarnitines are contained within the CNS and are unaffected by diet. (A and C) Concentrations of steady-state acylcarnitines were determined using approximately 25 mg of cortex tissue from 9-week-old $CPT2^{lox/lox}$ and $CPT2^{B-/-}$ mice given the control fed diet and after a 24-h fast ($n = 6$). (B and D) Additionally, steady-state acylcarnitines were determined using approximately 25 mg of cortex tissue from 18-week-old $CPT2^{lox/lox}$ and $CPT2^{B-/-}$ mice after 15 weeks on a low-fat or high-fat diet ($n = 6$). (E) Representative heat map images of charged mass acylcarnitine species and a phosphatidylcholine (PC K+) control from 50-μm-resolution MALDI IMS of 10-μm coronal brain slices from 24-h-fasted 6-month-old $CPT2^{lox/lox}$ ($n = 3$) and $CPT2^{B-/-}$ ($n = 3$) mice. The data are expressed as means and SEM. The data were analyzed using ordinary and repeated-measures two-way analysis of variance where appropriate, with Sidak tests for multiple comparisons. *, $\alpha = 0.05$; **, $\alpha = 0.01$; ***, $\alpha = 0.001$; ****, $\alpha = 0.0001$.

tine were unchanged by diet. Free carnitine was unchanged by diet, as well. Although nonsignificant, free carnitine was elevated in cortices of CPT2$^{B-/-}$ mice fed a low-fat diet compared to cortices of CPT2$^{lox/lox}$ mice (Fig. 6B).

As in hippocampus, long-chain ACs were dramatically elevated in CPT2$^{B-/-}$ cortex compared to CPT2$^{lox/lox}$ cortex, ranging from approximately 3- to over 20-fold in all dietary states, depending on the AC molecular species (Fig. 5C and 6C and D). In CPT2$^{B-/-}$ cortex, dietary conditions had a minimal effect on the steady-state concentrations of long-chain ACs. Long-chain AC species were largely unchanged by any diet in both CPT2$^{B-/-}$ and CPT2$^{lox/lox}$ cortices. However, linoleyl carnitine ($C_{18:2}$) was significantly elevated (2.27-fold) in the cortices of 24-h-fasted CPT2$^{B-/-}$ mice compared to cortices of fed CPT2$^{B-/-}$ mice (Fig. 6C). Steady-state concentrations of other, shorter ACs were decreased in the cortices of 24-h fasted CPT2$^{B-/-}$ mice compared to cortices of fed CPT2$^{B-/-}$ mice, including the following ACs: dodecenoyl carnitine ($C_{12:1}$), lauroyl carnitine ($C_{12:0}$), decanoic acid ($C_{10:0}$), and isovaleryl/2-methylbutyryl carnitine ($C_{5:0}$) (see Fig. S5A and B in the supplemental material). In the cortices of CPT2$^{B-/-}$ mice fed a high-fat diet, palmitoleyl carnitine ($C_{16:1}$) was significantly decreased in comparison to cortices of CPT2$^{B-/-}$ mice fed a low-fat diet (Fig. 6D). In summary, diet and fasting had a minimal effect on the steady-state concentrations of ACs regardless of chain length, suggesting that the brain oxidizes fatty acids independently of elevated blood lipoprotein or free fatty acid concentrations. The minimal contributions of diet to acylcarnitine concentrations in the brain may be due to the rate of passage of dietary fatty acids across the BBB. When supplied with 100 μM oleate, primary astrocytes from CPT2$^{B-/-}$ mice expelled nearly three times as much oleylcarnitine ($C_{18:1}$) into media (see Fig. S5E).

To explore the regional distribution of ACs throughout different regions of the brain, we performed matrix-assisted laser desorption ionization imaging mass spectrometry (MALDI IMS), with the Applied Imaging Mass Spectrometry (AIMS) core facility at Johns Hopkins School of Medicine, at 50-μm resolution using representative 10-μm coronal slices, ~3.5 mm from the anterior of the brain, which represented brain regions including parts of the cortex, hippocampus, midbrain, and some cerebellum on a single slice. The sample brains were from 24-h-fasted adult CPT2$^{lox/lox}$ and CPT2$^{B-/-}$ mice to determine the spatial resolution of metabolites after FAO deletion in the brain. The representative coronal sections described above allowed comparison of metabolites throughout the brain (Fig. 6E). In representative heat maps of charged ions that correspond to selected ACs, we observed ubiquitously increased abundances of $C_{16:0}$, $C_{16:1}$, $C_{18:1}$, and $C_{18:3}$ ACs throughout all brain regions in CPT2$^{B-/-}$ coronal slices compared to CPT2$^{lox/lox}$ slices, while ionized phosphatidylcholines (PC K^+) remained unchanged between the two slices from both genotypes (Fig. 6E). These data further validate the increase in long-chain ACs in CPT2$^{B-/-}$ brains.

We have observed elevated long-chain ACs in both hippocampi and cortices of CPT2$^{B-/-}$ mice across several dietary and physiological conditions (Fig. 5C and 6). While we explored a potential systemic impact on serum metabolites, such as triacylglycerols, ketones, and nonesterified fatty acids (NEFAs), we have not discerned how the loss of CNS long-chain FAO impacts serum ACs. The systemic steady-state blood AC concentration going toward the brain and the steady-state blood AC concentration coming from the brain were measured in common carotid arteries (systemic blood going to the brain) and jugular veins (blood coming from the brain) of fed 11-week-old male CPT2$^{B-/-}$ and CPT2$^{lox/lox}$ mice. We hypothesized that we might observe an efflux of long-chain ACs from the brain via the CPT2$^{B-/-}$ jugular vein due to observed accumulations of long-chain ACs in brain tissue (Fig. 5C and 6). A comparison of total ACs between genotypes showed no significant difference in steady-state concentrations of total ACs from arterial blood between CPT2$^{B-/-}$ and CPT2$^{lox/lox}$ mice. Total ACs from venous blood were significantly decreased in CPT2$^{B-/-}$ compared to CPT2$^{lox/lox}$ mice. Free carnitine and acetylcarnitine were both decreased in CPT2$^{B-/-}$ blood compared to CPT2$^{lox/lox}$ blood from both common carotid arteries and jugular veins (Fig. 7A).

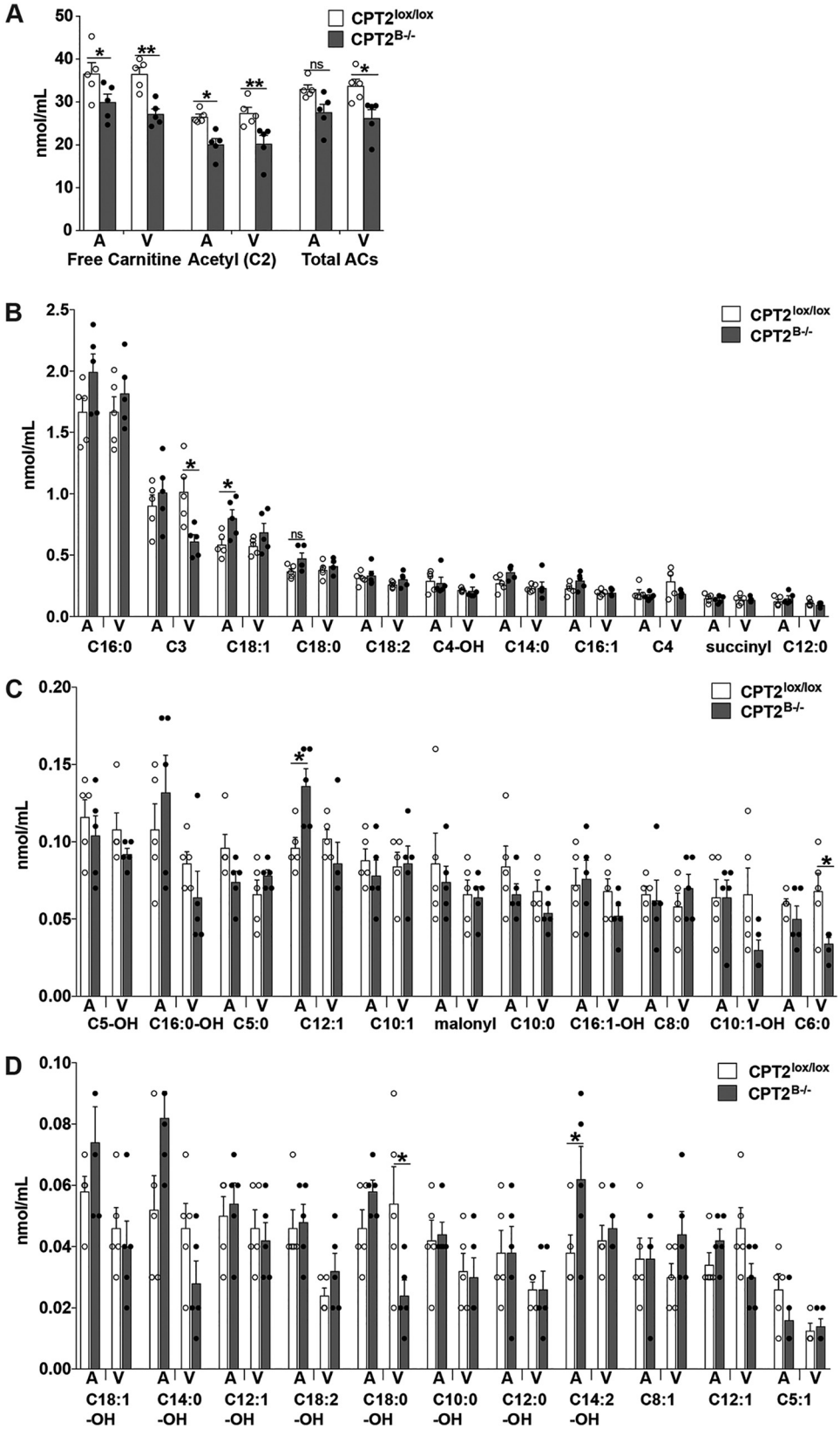

FIG 7 Long-chain acylcarnitines elevated in CPT2$^{B-/-}$ mouse hippocampus and cortex are contained within the CNS and not delivered from the brain into the blood. Abundances of acylcarnitines were determined from dried blood spots collected from common carotid arteries and external jugular veins from CPT2$^{lox/lox}$ and CPT2$^{B-/-}$ mice fasted for 4 h immediately prior to blood collection ($n = 5$). Abundances of individual acylcarnitine species in

(Continued on next page)

When examining individual AC species, there were few long-chain AC species that had significant differences in concentration attributed to genotype in either arterial or venous blood. In arterial blood, oleic acid ($C_{18:1}$) was elevated in CPT2$^{B-/-}$ mice compared to CPT2$^{lox/lox}$ mice. In venous blood, 3-hydroxyoleic acid ($C_{18:1}$-OH) was depleted 2.25-fold in CPT2$^{B-/-}$ blood compared to CPT2$^{lox/lox}$ blood (Fig. 7B). Several shorter AC species were significantly altered in both arterial and venous blood on the basis of genotype. Both myristoleic ($C_{14:1}$) and tetradecadienoyl ($C_{14:2}$) carnitines were significantly elevated in arterial CPT2$^{B-/-}$ blood compared to arterial CPT2$^{lox/lox}$ blood. In venous blood, propioyl (C_3) and capronyl ($C_{6:0}$) carnitines were decreased 1.67-fold and 2-fold, respectively, in CPT2$^{B-/-}$ blood compared to CPT2$^{lox/lox}$ blood (Fig. 7B to D). However, none of these significant results were the result of a substantial effect size, nor were there stereotyped differences on the basis of genotype in classes of AC species. Therefore, these data suggest that the substrates and products of FAO are relatively confined within the BBB.

DISCUSSION

In this study, we demonstrated evidence for the existence of robust FAO within mammalian brains under normal circumstances. Intermediates were confined largely within the BBB, and oxidation was not influenced by the dietary state, using a straightforward and stringent genetic model. Previous studies showed that the brain expresses mitochondrial β-oxidation and carnitine shuttle system enzymes over the course of development, throughout multiple brain regions, and primarily in astrocytes (17–19). Studies have also found that isolated brain mitochondria (23, 24), cultured astrocytes (21, 22), *ex vivo* brain tissue (17), and *in vivo* rodents (25) are all capable of oxidizing exogenous [^{14}C]palmitic acid/or [^{14}C]oleic acid to $^{14}CO_2$. In our model, impairment of FAO in the brain is followed by an inability to oxidize radiolabeled lipid in cultured astrocytes and stark changes in the brain metabolome in tissue. Most notably, high accumulations of ACs in brain tissue are evidence that long-chain FAs are mobilized in the mitochondria for β-oxidation under normal conditions and result in the accumulation of long-chain ACs in hippocampus and cortex after the loss of CPT2.

Hepatic FAO is required for ketogenesis in the liver (49). Liver-generated ketones are a major energy substrate in the CNS in a fasted state following the suppression of circulating glucose, during early postnatal development, and under stress conditions (1, 57). Hepatic ketones delivered to the brain are required to sustain brain β-hydroxybutyrate in the fasted state. In 24-h-fasted mice incapable of hepatic FAO, β-hydroxybutyrate was depleted in the hippocampus. However, in CPT2$^{B-/-}$ fasted-mouse hippocampus, β-hydroxybutyrate abundance remained constant. While past studies showed that astrocytes are capable of *de novo* ketogenesis, our data show that the majority of ketones in the brain are not generated *de novo* but instead are supplied by the liver (20, 21, 52).

FA concentrations in the brain are dependent on dietary intake (58, 59). Studies have also shown that *de novo* ketogenesis in astrocytes is stimulated by a high-fat diet (60). However, in our study, systemic changes in metabolism due to diet did not impact long-chain FAO in the brain, likely due to the rate of passage of FAs across the BBB. However, increased ACs were observed in media from primary astrocytes derived from brain FAO KO mice. Additionally, long-chain ACs that accumulate as a result of CPT2 loss are retained in the brain, possibly due to the BBB. CNS-accumulated ACs are not readily expelled into the bloodstream, nor does brain CPT2 loss result in systemic increases in blood ACs. These data suggest that FAO in the brain occurs with minimal influence from or impact on peripheral tissues.

Evidence from our study suggests a larger capacity and potentially a larger role for

FIG 7 Legend (Continued)
arterial and venous blood from 4-h-fasted adult mice are shown. The data are expressed as means and SEM. The data were analyzed using repeated-measures two-way analysis of variance with Sidak tests for multiple comparisons. *, $\alpha = 0.05$; **, $\alpha = 0.01$; ns, not significant.

FAO within the mammalian brain than once considered. This study supports the significance of exploring other questions in FA neurometabolism in future studies, including cross talk with the neuron functional role(s) and regulation of FAO in the brain by metabolic cues. Our study and others suggest that mitochondrial β-oxidation in the brain is largely astrocytic based on the expression and catalytic activities of β-oxidation enzymes and on lipid oxidation studies using labeled lipid (17, 18, 21, 22, 33). However, lipids play numerous substantial yet varied roles in neurons. Hypothalamic lipid-sensing neurons, outside of the BBB, are capable of rapid inhibitory effects on liver glucose homeostasis (41, 42); neuron-associated channel proteins are regulated by lipid (41, 42); and neurons have a unique lipid composition in cell membranes with elevated PUFAs, such as docosahexaenoic acid (DHA) (31, 61). Interestingly, the capacity for FAO is considered miniscule to negligible in neurons. In addition to decreased expression of β-oxidation enzymes compared to astrocytes, neurons specifically express acyl-CoA thioesterase 7 (*Acot7* product). In order to be retained within cells, FAs require esterification to CoA, yielding acyl-CoAs. ACOT7 protein is highly abundant in neuronal cytosol and regulates FA retention in neurons by specifically hydrolyzing acyl-CoAs, thereby evicting FAs from neurons for use in astrocytes (29). While other groups have suggested that FAs are packaged and shuttled from neurons to astrocytes during times of high activity (32), no evidence regarding whether this occurs under normal conditions with endogenous lipid exists.

Genes related to β-oxidation are important for proper brain morphology and function. CPT1c is a brain-specific homolog of CPT1 (62). Unlike CPT1a, CPT1c protein does not exhibit catalytic acyltransferase activity *in vitro*, nor does it contribute to the β-oxidation of long-chain FAs (63–65). CPT1c KO mice do not phenocopy CPT2$^{B-/-}$ mice, further demonstrating the lack of a role of CPT1c in β-oxidation (65, 66). However, CPT1c plays a role in regulating food intake and energy expenditure by binding neuronal malonyl-CoA (64, 67, 68) When conditionally overexpressed in mouse brain, CPT1c results in postnatal microencephaly and a diet-dependent depletion of very long-chain FAs, which suggests CPT1c has a potentially broader role in neurometabolism (37). The role of FA metabolism in neurodevelopment mentioned above may also be observed upon overexpression of the canonical carnitine shuttle proteins CPT1a and CPT2. Although in the present study loss of CPT2 in the brain did not affect brain volume and had a minimal impact on gross brain anatomy, it did lead to major and unexpected changes in the brain metabolome, supporting the importance of FAO within the CNS.

While the brain is canonically known to use glucose as its primary energy substrate, we showed that the mammalian CNS oxidizes long-chain fatty acids under normal conditions. Loss of β-oxidation in the brain resulted in a minor decrease in middle-zone exploration and a potential social memory deficit but did not result in a major overt behavioral phenotype. Loss of FAO in the brain leads to evenly distributed accumulations of long-chain ACs in multiple brain regions, among other changes to the brain metabolome. By-products of long-chain FA β-oxidation within the CNS are confined to brain tissue, and FAO in the brain is not modulated by diet. Regardless of any possible undetermined functional role(s), whether for turnover of cell membrane lipid or for use as an energetic substrate, FAO exists in the mammalian brain under normal conditions.

MATERIALS AND METHODS

Animals. All procedures were performed in accordance with the NIH's Guide for the Care and Use of Laboratory Animals and under the approval of the Johns Hopkins Medical School Animal Care and Use Committee.

To generate mice with pan-brain-specific loss of function of long-chain FAO (CPT2$^{B-/-}$ mice), we bred CPT2$^{lox/lox}$ mice (36) to nestin-Cre transgenic mice (37). For one set of behavioral testing, CPT2$^{B-/-}$ mice were crossed with wild-type mice to generate CPT2$^{lox/+}$ nestin-Cre mice. The mice were housed in ventilated racks with a 14-h light/10-h dark cycle and fed a standard chow diet (2018SX; Teklad Global). Fed and 24-h-fasted mice were euthanized at the same time of day (3 p.m.) at 9 weeks of age unless otherwise noted. For fasting studies, mice were deprived of food for 24 h (3 p.m. to 3 p.m.). The food deprivation schedule and timing of tissue collection were consistent for CPT2$^{L-/-}$ mice (49, 50) and PPAR$\alpha^{-/-}$ mice (Jackson Laboratories; stock no. 008154).

For diet studies, CPT2$^{lox/lox}$ and CPT2$^{B-/-}$ mice were fed either a 60% HFD (D12492; Research Diets) or an LFD (D12450J; Research Diets) starting at 3 weeks of age and continuing for 15 weeks. Serum was collected from LFD and HFD CPT2$^{lox/lox}$ and CPT2$^{B-/-}$ mice to measure free glycerol and triacylglycerol (TAG) (both also measured in cortex homogenates) (Sigma), β-hydroxybutyrate (also measured in cortex homogenates) (StanBio), and total cholesterol and NEFA (Wako). Lipid peroxidation was measured using a TBARS assay kit (Cayman Chemical Company) in brain tissue homogenates as previously described (36). The LFD and HFD mice were euthanized at 18 weeks of age, and tissues were collected.

Primary astrocyte isolation and culture. T-25 culture flasks (Falcon; 353109; one per cortex) were coated with 1:500 rat tail collagen I (ThermoFisher; A1048301) in Dulbecco's modified Eagle medium (DMEM) for 4 h. Afterward, the culture flasks were washed with 1× phosphate-buffered saline (PBS) (Quality Biological) and set to dry. Brains from P2 CPT2$^{lox/lox}$ and CPT2$^{B-/-}$ mice were rapidly dissected in ice-cold 1× Hanks buffered salt solution (HBSS) (no Ca^{2+} or Mg^{2+}; ThermoFisher). The hippocampus, midbrain, cerebellum, and brainstem from each cortex were discarded, and the meninges were completely removed. On ice, the cortex tissue in 1× HBSS was gently minced using sterile razor blades. The minced cortex and 4 ml of HBSS were recovered and transferred to 14-ml round-bottom culture tubes. One milliliter of 0.25% trypsin-EDTA was added to each round-bottom tube, and the tubes were gently shaken for 25 min at 37°C. The cortices were washed twice with DMEM, 15% fetal bovine serum, and 1% penicillin-streptomycin antibiotic (Invitrogen) to remove the trypsin-EDTA (ThermoFisher). The tissues were dissociated by gently triturating them using a 2-ml sterile serological pipette, followed by three subsequent triturations using a sterile Pasteur pipette. The supernatant from each round of trituration was transferred to a new round-bottom tube. The cell suspension was passed through a 40-μM cell strainer and resuspended in 5 ml of DMEM, 15% fetal bovine serum, and 1% penicillin-streptomycin antibiotic (Invitrogen) on coated T-25 flasks. The medium of each flask was changed every 2 or 3 days. The astroglia grew to confluence within 10 to 14 days.

Fatty acid oxidation, glucose oxidation, and glucose uptake. All labeling experiments were performed using P2 primary cortical astrocytes from CPT2$^{lox/lox}$ and CPT2$^{B-/-}$ pups seeded in 1:500 rat collagen (ThermoFisher; A1048301)-coated T-25 flasks or 6-well culture dishes 48 h prior to the experiment. All assays were conducted between passages 2 and 4. For FAO experiments (the protocol was modified from reference 17), 200,000 astrocytes per flask were labeled in stoppered T-25 flasks with labeling medium containing 0.12 μCi [1-^{14}C]oleic acid (Moravek Biochemicals, Brea, CA) and incubated at 37°C (5% CO_2; 90% relative humidity) for 4 h. The labeling medium was composed of 20% neurobasal medium (Gibco; 21103-049) and 80% glucose-, glutamine-, and pyruvate-free DMEM (Gibco; A14430) supplemented so that the final concentrations were 5 mM glucose, 25 μM glutamine, 50 μM sodium pyruvate, 0.2 mM carnitine, and 0.1% (wt/vol) bovine serum albumin (Sigma; A9647). Etomoxir-treated samples were incubated in 100 μM etomoxir (Sigma; E1905) in the labeling medium administered at the time of initiating the assay. $^{14}CO_2$ was trapped on Whatman filter paper suspended in the headspace of the flask using a center well by addition of 200 μl of 70% perchloric acid in the medium and 150 μl of 1 M NaOH directly on the filter paper and incubation at 55°C for 1 h. The filter paper was placed in 4 ml of scintillation fluid, and the radioactivity was measured. The astrocytes were lysed using 0.5 ml 1× Triton X-100 in 1× PBS. Counts were normalized to total micrograms of protein determined by bicinchoninic acid (BCA) assay. Glucose oxidation was performed as previously described using [U-^{14}C]glucose and approximately 30 mg of brain explant tissue from CPT2$^{lox/lox}$ and CPT2$^{B-/-}$ adults (29). Glucose uptake was measured using modified well-established protocols (17, 69). Astrocytes (200,000 per flask) were labeled in 6-well culture dishes with labeling medium containing 0.2 μCi [1-^{3}H]2-deoxy-D-glucose (Moravek Biochemicals, Brea, CA) and incubated at 37°C (5% CO_2; 90% relative humidity) for 4 h. The labeling medium was composed of 20% neurobasal medium (Gibco; 21103-049) and 80% glucose-, glutamine-, and pyruvate-free DMEM (Gibco; A14430) supplemented so that the final concentrations were 5 mM glucose, 25 μM glutamine, and 50 μM sodium pyruvate. Each culture was thoroughly washed in ice-cold 1× PBS. The cultures were dissolved in 600 μl of 1 M NaOH overnight at room temperature, transferred to Eppendorf tubes, vortexed, and centrifuged at high speed for 30 min. The radioactivity from 150 μl of lysate was counted in 4 ml of scintillation fluid and normalized to total micrograms of protein as determined by BCA assay.

Acylcarnitines (cortex, blood, and primary astrocyte media). Cortical acylcarnitines were prepared using well-described methods with modifications (17). Cortex was rapidly dissected and frozen on liquid nitrogen. Approximately 25 mg of prefrontal cortex was cut from each sample and weighed on dry ice for subsequent analysis. The frozen cortex was homogenized in methanol solution containing internal standards of acylcarnitines (NSK B; Cambridge Isotopes), sonicated for 10 min at 20 to 25°C, and centrifuged for 4 min at 15,520 rpm at 4°C. Following centrifugation, the liquid phase was transferred to a clean glass tube and evaporated to dryness under nitrogen. The dried samples were resuspended by adding 60 μl 3 N HCl in *n*-butanol. The samples were incubated for 15 min at 65°C and, following incubation, evaporated under nitrogen. Butylated acylcarnitines were reconstituted in 100 μl of mobile phase acetonitrile-water-formic acid (H_2O-CH_3CN-HCOOH; 80:19.9;0.1 [vol/vol/percent]). Samples were vortexed, transferred to a centrifuge filter, and spun. The filtrates obtained were transferred to injection vials.

Blood acylcarnitine concentrations were quantified using a well-established method of testing dried blood spots (DBSs), with modifications, as previously described (17, 49). Blood was collected from external jugular veins and common carotid arteries of 11-week-old CPT2$^{lox/lox}$ and CPT2$^{B-/-}$ mice beginning at 10 a.m. after 4 h of food deprivation (6 a.m. to 10 a.m.) to correct for inconsistent feeding patterns. The mice were anesthetized using a regulated flow of isoflurane and were immediately euthanized following the procedure. Punched 1/8-in DBS samples were submerged in 100 μl of meth-

anol solution containing internal standards for acylcarnitines (NSK B; Cambridge Isotopes). The samples were incubated at 4°C for 20 min and dried under liquid nitrogen, and then 60 μl 3 N HCl in *n*-butanol was added. The samples were incubated for 15 min at 65°C and then dried under liquid nitrogen, and butylated acylcarnitines were reconstituted in 100 μl of mobile phase acetonitrile-water-formic acid (H_2O-CH_3CN-HCOOH; 80:19.9:0.1 [vol/vol/percent]). The samples were vortexed, transferred to a centrifuge filter, spun, and transferred to an injection vial.

Acylcarnitines were quantified from media derived from primary P2 cultured CPT2$^{lox/lox}$ and CPT2$^{B-/-}$ mice. Oleate medium (100 μM) was composed of 20% neurobasal medium (Gibco; 21103-049) and 80% glucose-, glutamine-, and pyruvate-free DMEM (Gibco; A14430) supplemented so that the final concentrations were 100 μM oleate, 5 mM glucose, 25 μM glutamine, 50 μM sodium pyruvate, 0.2 mM carnitine, and 0.1% (wt/vol) bovine serum albumin (Sigma; A9647). Primary astrocytes were incubated in 100 μM oleate overnight prior to medium collection and prepared as described above.

Unbiased global metabolomics. Global metabolomics were performed on rapidly dissected and frozen (in liquid nitrogen) hippocampi from 24-h-fasted (3 p.m. to 3 p.m.) 9-week-old mice as described previously (29, 66, 70, 71).

RNA isolation, purification, and qRT-PCR. RNA was isolated from brain tissues using TRIzol (Life Technologies, Grand Island, NY) and further purified using an RNeasy minikit (Qiagen, Valencia, CA). RNA was quantified with a NanoDrop spectrophotometer (ThermoFisher Scientific, Madison, WI), and cDNA was synthesized using 0.5 to 2 μg of total RNA, random primers, and a MultiScribe high-capacity cDNA reverse transcription kit (Life Technologies; catalog no. 4368814) according to the manufacturer's instructions. Quantitative real-time PCR (qRT-PCR) was performed using 10 ng of template cDNA and Bio-Rad (Hercules, CA) SsoAdvanced universal SYBR green master mix (catalog no. 1725274) with primers specific for the genes of interest (see Table S2 in the supplemental material). PCRs were carried out in a Bio-Rad CFX Connect thermocycler (95°C for 10 s and 56°C to 95°C at 0.5°C/5 s). All data were normalized to the average of housekeeping threshold cycle (C_T) values from Rpl22 and 18S. Normalized data were expressed as $2^{-\Delta CT}$.

Behavioral testing. All behavioral testing was performed in the light part of the light/dark cycle. Behavioral testing included open-field, social recognition memory task, and rotarod tests, as described below. The behavioral tasks were separated by at least 24 h, and animals were returned to their home cages at the end of each day. All experiments were recorded and quantified by a trained observer blinded to the genotype of the mice, using AnyMaze equipment and software (open-field and social recognition tests) and a Rotamex apparatus (Columbus Instruments, Columbus, OH) (rotarod).

(i) Open-field testing. Open-field testing was modified from previous studies (12, 45). Testing was carried out in a square open-field arena (AnyMaze box; 40 cm by 40 cm) under indirect diffuse room light. Each animal was placed in the arena and observed for 5 min. Activity measures included total distance traveled, percent time spent in active exploration (episodes of movement at $\geq$5 cm/s), and speed of movement during the active exploration. To assess anxiety levels, the activity measures in different zones were quantified, since mice have a natural predilection to be near a wall (46). Specifically, the arena was divided into three zones: inner, middle, and outer. After each trial, the chamber was cleaned with a damp towel, followed by 70% alcohol.

(ii) Social recognition memory task. The social recognition memory task was carried out in the open-field arena by placing a mouse inside a standard mouse cage as previously described (5, 48). The 12-week-old female test mouse was exposed to the same juvenile mouse (postnatal day 21) for 2 min over 2 trials with interinterval gaps of 20 min. For the third trial, the test mouse was exposed to a new juvenile mouse from a different litter for 2 min. The time spent in social investigation (direct, active olfactory exploration, i.e., sniffing and nosing head and anogenital areas, following, and pursuit) was quantified. A decrease in time between trials 1 and 2 reflected social habituation, while an increase from trial 2 to trial 3 was a measure of dishabituation.

(iii) Rotarod testing. The rotarod test was used to assess balance, coordination, and fatigue. Mice were tested at 12 weeks of age using a Rotamex apparatus (Columbus Instruments, Columbus, OH) as previously described (72–74). In brief, on day 1, the mice performed habituation trials by being placed on a rotarod at 4 rpm for 60 s. On day 2, each mouse had two trials; each trial lasted for 10 min with 60-min intertrial intervals. During the trials, the rotarod accelerated from 4 rpm to 40 rpm. Latency to fall from the rotarod was quantified. After each trial, the Rotamex apparatus was cleared of feces and urine using a damp paper towel and 70% alcohol and allowed to air dry.

MRI. *Ex vivo* MRI was performed on the heads of adult female CPT2$^{lox/lox}$ and CPT2$^{B-/-}$ mice after exsanguination by perfusion with saline. The *ex vivo* MRI was performed on a vertical 9.4-T nuclear magnetic resonance (NMR) spectrometer with a volume coil (15-mm diameter; Bruker Biospin, Billerica, MA) as a radiofrequency transmitter and receiver. The diffusion tensor magnetic resonance imaging (DTI) data were acquired using diffusion-weighted gradient echo and spin echo (dwGRASE) sequence with the following parameters: 9 diffusion-weighted images with a *b* value of 1,100, in addition to two minimally diffusion-weighted images; TR/TE = 800/33.3 ms; resolution = 0.125 mm by −0.125 mm; field of view (fov) = 16 mm by 9 mm by 18 mm. The total imaging time was approximately 9 h. Three-dimensional T2-weighted images were acquired with the same field of view and resolution using fast-spin echo sequence, with a TE/TR ratio of 40/2,000 ms, a flip angle of 180°, four signal averages, an echo train length of 8, and an imaging time of about 3 h. Brain regional and total volume measurements were performed using ROIEditor (http://www.mristudio.org) and an in-house-built atlas. We manually defined corpus collosum (entire genu) in the fractional anisotropy images using ROIEditor and obtained the average fractional anisotropy value in the individual subjects as in previous studies (75–77).

MALDI-IMS. MALDI-IMS was acquired in the Applied Imaging Mass Spectrometry Core/Service Center at Johns Hopkins using 10-μm coronal slices, approximately 3.5 mm from the posterior of the brain, from the brains of 24-h-fasted adult CPT2$^{lox/lox}$ and CPT2$^{B-/-}$ mice (6 months old). All slices to be compared were prepared on a single slide for simultaneous acquisition at 50-μm resolution using a Bruker Rapiflex MALDI-time of flight (TOF)/TOF instrument. The slides were sprayed with 5 mg/ml 4-chloro-alpha-cyanocinnamic acid with a 70% acetonitrile and 2% trifluoroacetic acid solution. Data were processed and heat map images were generated using SCiLS software (https://scils.de).

Statistical analysis. Data were analyzed using Prism 7.0 software (GraphPad). The statistical significance of the data was determined using unpaired Student two-tailed *t* tests for single-variable experiments. For unmatched multiple-variable experiments, ordinary two-way analysis of variance (ANOVA) with Sidak corrections for multiple comparisons was used to determine the statistical significance of the data. For paired multiple-variable experiments, repeated-measures two-way ANOVA with Sidak corrections for multiple comparisons was used to determine the statistical significance of the data.

SUPPLEMENTAL MATERIAL

Supplemental material is available online only.

SUPPLEMENTAL FILE 1, PDF file, 3.6 MB.

SUPPLEMENTAL FILE 2, XLSX file, 0.01 MB.

SUPPLEMENTAL FILE 3, XLSX file, 0.3 MB.

ACKNOWLEDGMENTS

This work was supported in part by National Institutes of Health (NIH) grants R01NS072241 to M.J.W., R01NS110808 and R01NS111230 to S.S., and F31NS102151 to C.J.W. C.J.W. was additionally supported by NIH grant T32GM007445, awarded to the Biochemistry, Cellular and Molecular Biology Graduate Program at Johns Hopkins School of Medicine.

We thank the Johns Hopkins Applied Imaging Mass Spectrometry (AIMS) Core Facility at the Johns Hopkins University School of Medicine for undertaking the MALDI imaging in this project.

We have no competing financial interests.

C.J.W., J.L., J.C., S.S., T.C., and M.J.W. performed experiments and wrote the manuscript.

REFERENCES

1. Owen OE, Morgan AP, Kemp HG, Sullivan JM, Herrera MG, Cahill GF, Jr. 1967. Brain metabolism during fasting. J Clin Invest 46:1589–1595. https://doi.org/10.1172/JCI105650.
2. Ahmed AT, Mahmoudian Dehkordi S, Bhattacharyya S, Arnold M, Liu D, Neavin D, Moseley MA, Thompson JW, John Williams LS, Louie G, Skime MK, Wang L, Riva-Posse P, McDonald W, Bobo WV, Craighead WE, Krishnan R, Weinshilboum RM, Dunlop BW, Millington DS, Rush AJ, Frye MA, Kaddurah-Daouk R. 2019. Acylcarnitine metabolomic profiles inform clincally-defined major depressive phenotypes. bioRxiv https://doi.org/10.1101/632448.
3. Barone R, MIMIC-Autism Group, Alaimo S, Messina M, Pulvirenti A, Bastin J, Ferro A, Frye RE, Rizzo R. 2018. A subset of patients with autism spectrum disorders show a distinctive metabolic profile by dried blood spot analyses. Front Psychiatry 9:636. https://doi.org/10.3389/fpsyt.2018.00636.
4. Clark-Taylor T, Clark-Taylor BE. 2004. Is autism a disorder of fatty acid metabolism? Possible dysfunction of mitochondrial beta-oxidation by long chain acyl-CoA dehydrogenase. Med Hypotheses 62:970–975. https://doi.org/10.1016/j.mehy.2004.01.011.
5. Ferguson JN, Young LJ, Insel TR. 2002. The neuroendocrine basis of social recognition. Front Neuroendocrinol 23:200–224. https://doi.org/10.1006/frne.2002.0229.
6. Rossignol DA, Frye RE. 2012. Mitochondrial dysfunction in autism spectrum disorders: a systematic review and meta-analysis. Mol Psychiatry 17:290–314. https://doi.org/10.1038/mp.2010.136.
7. Xie Z, Jones A, Deeney JT, Hur SK, Bankaitis VA. 2016. Inborn errors of long-chain fatty acid beta-oxidation link neural stem cell self-renewal to autism. Cell Rep 14:991–999. https://doi.org/10.1016/j.celrep.2016.01.004.
8. Tyni T, Palotie A, Viinikka L, Valanne L, Salo MK, von Döbeln U, Jackson S, Wanders R, Venizelos N, Pihko H. 1997. Long-chain 3 hydroxyacyl-coenzyme A dehydrogenase deficiency with the G158C mutation clinical presentation of thirteen patients. J Pediatr 130:67–76. https://doi.org/10.1016/S0022-3476(97)70312-3.
9. Tyni T, Pihko H. 1999. Long-chain 3-hydroxyacyl-CoA dehydrogenase deficiency. Acta Paediatr 88:237–245. https://doi.org/10.1080/08035259950169954.
10. Merritt JL, II, Norris M, Kanungo S. 2018. Fatty acid oxidation disorders. Ann Transl Med 6:473. https://doi.org/10.21037/atm.2018.10.57.
11. Cahill GF, Jr. 2006. Fuel metabolism in starvation. Annu Rev Nutr 26:1–22. https://doi.org/10.1146/annurev.nutr.26.061505.111258.
12. Lopatina O, Yoshihara T, Nishimura T, Zhong J, Akther S, Fakhrul AA, Liang M, Higashida C, Sumi K, Furuhara K, Inahata Y, Huang JJ, Koizumi K, Yokoyama S, Tsuji T, Petugina Y, Sumarokov A, Salmina AB, Hashida K, Kitao Y, Hori O, Asano M, Kitamura Y, Kozaka T, Shiba K, Zhong F, Xie MJ, Sato M, Ishihara K, Higashida H. 2014. Anxiety- and depression-like behavior in mice lacking the CD157/BST1 gene, a risk factor for Parkinson's disease. Front Behav Neurosci 8:133. https://doi.org/10.3389/fnbeh.2014.00133.
13. Camargo N, Brouwers JF, Loos M, Gutmann DH, Smit AB, Verheijen MH. 2012. High-fat diet ameliorates neurological deficits caused by defective astrocyte lipid metabolism. FASEB J 26:4302–4315. https://doi.org/10.1096/fj.12-205807.
14. Polyzos AA, Lee DY, Datta R, Hauser M, Budworth H, Holt A, Mihalik S, Goldschmidt P, Frankel K, Trego K, Bennett MJ, Vockley J, Xu K, Gratton E, McMurray CT. 2019. Metabolic reprogramming in astrocytes distinguishes region-specific neuronal susceptibility in Huntington mice. Cell Metab 29:1258–1273 e11. https://doi.org/10.1016/j.cmet.2019.03.004.
15. Mitchell RW, Hatch GM. 2011. Fatty acid transport into the brain: of fatty acid fables and lipid tails. Prostaglandins Leukot Essent Fatty Acids 85:293–302. https://doi.org/10.1016/j.plefa.2011.04.007.
16. Watkins PA, Hamilton JA, Leaf A, Spector AA, Moore SA, Anderson RE, Moser HW, Noetzel MJ, Katz R. 2001. Brain uptake and utilization of fatty acids: applications to peroxisomal biogenesis diseases. J Mol Neurosci 16:87–92. https://doi.org/10.1385/JMN:16:2-3:87.

17. Jernberg JN, Bowman CE, Wolfgang MJ, Scafidi S. 2017. Developmental regulation and localization of carnitine palmitoyltransferases (CPTs) in rat brain. J Neurochem 142:407–419. https://doi.org/10.1111/jnc.14072.
18. Clarke LE, Liddelow SA, Chakraborty C, Munch AE, Heiman M, Barres BA. 2018. Normal aging induces A1-like astrocyte reactivity. Proc Natl Acad Sci U S A 115:E1896–E1905. https://doi.org/10.1073/pnas.1800165115.
19. Fecher C, Trovo L, Muller SA, Snaidero N, Wettmarshausen J, Heink S, Ortiz O, Wagner I, Kuhn R, Hartmann J, Karl RM, Konnerth A, Korn T, Wurst W, Merkler D, Lichtenthaler SF, Perocchi F, Misgeld T. 2019. Cell-type-specific profiling of brain mitochondria reveals functional and molecular diversity. Nat Neurosci 22:1731–1742. https://doi.org/10.1038/s41593-019-0479-z.
20. Le Foll C, Levin BE. 2016. Fatty acid-induced astrocyte ketone production and the control of food intake. Am J Physiol Regul Integr Comp Physiol 310:R1186–R1192. https://doi.org/10.1152/ajpregu.00113.2016.
21. Auestad N, Korsak RA, Morrow JW, Edmond J. 1991. Fatty acid oxidation and ketogenesis by astrocytes in primary culture. J Neurochem 56:1376–1386. https://doi.org/10.1111/j.1471-4159.1991.tb11435.x.
22. Edmond J, Robbins RA, Bergstrom JD, Cole RA, de Vellis J. 1987. Capacity for substrate utilization in oxidative metabolism by neurons, astrocytes, and oligodendrocytes from developing brain in primary culture. J Neurosci Res 18:551–561. https://doi.org/10.1002/jnr.490180407.
23. Vignais PM, Gallagher CH, Zabin I. 1958. Activation and oxidation of long chain fatty acids by rat brain. J Neurochem 2:283–287. https://doi.org/10.1111/j.1471-4159.1958.tb12375.x.
24. Kawamura N, Kishimoto Y. 1981. Characterization of water-soluble products of palmitic acid beta-oxidation by a rat brain preparation. J Neurochem 36:1786–1791. https://doi.org/10.1111/j.1471-4159.1981.tb00432.x.
25. Gnaedinger JM, Miller JC, Latker CH, Rapoport SI. 1988. Cerebral metabolism of plasma [^{14}C]palmitate in awake, adult rat: subcellular localization. Neurochem Res 13:21–29. https://doi.org/10.1007/bf00971850.
26. Yang SY, He X, Schulz H. 1987. Fatty acid oxidation in rat brain is limited by the low activity of 3-ketoacyl-coenzyme A thiolase. J Biol Chem 262:13027–13032.
27. Wegener G. 1983. Brains burning fat: different forms of energy metabolism in the CNS of insects. Naturwissenschaften 70:43–45. https://doi.org/10.1007/bf00365961.
28. Cermenati G, Audano M, Giatti S, Carozzi V, Porretta-Serapiglia C, Pettinato E, Ferri C, D'Antonio M, De Fabiani E, Crestani M, Scurati S, Saez E, Azcoitia I, Cavaletti G, Garcia-Segura L-M, Melcangi RC, Caruso D, Mitro N. 2015. Lack of sterol regulatory element binding factor-1c imposes glial fatty acid utilization leading to peripheral neuropathy. Cell Metab 21:571–583. https://doi.org/10.1016/j.cmet.2015.02.016.
29. Ellis JM, Wong GW, Wolfgang MJ. 2013. Acyl coenzyme A thioesterase 7 regulates neuronal fatty acid metabolism to prevent neurotoxicity. Mol Cell Biol 33:1869–1882. https://doi.org/10.1128/MCB.01548-12.
30. Escartin C, Pierre K, Colin A, Brouillet E, Delzescaux T, Guillermier M, Dhenain M, Deglon N, Hantraye P, Pellerin L, Bonvento G. 2007. Activation of astrocytes by CNTF induces metabolic plasticity and increases resistance to metabolic insults. J Neurosci 27:7094–7104. https://doi.org/10.1523/JNEUROSCI.0174-07.2007.
31. Schonfeld P, Reiser G. 2017. Brain energy metabolism spurns fatty acids as fuel due to their inherent mitotoxicity and potential capacity to unleash neurodegeneration. Neurochem Int 109:68–77. https://doi.org/10.1016/j.neuint.2017.03.018.
32. Ioannou MS, Jackson J, Sheu SH, Chang CL, Weigel AV, Liu H, Pasolli HA, Xu CS, Pang S, Matthies D, Hess HF, Lippincott-Schwartz J, Liu Z. 2019. Neuron-astrocyte metabolic coupling protects against activity-induced fatty acid toxicity. Cell 177:1522–1535 e14. https://doi.org/10.1016/j.cell.2019.04.001.
33. Guest J, Garg M, Bilgin A, Grant R. 2013. Relationship between central and peripheral fatty acids in humans. Lipids Health Dis 12:79. https://doi.org/10.1186/1476-511X-12-79.
34. Ouellet M, Emond V, Chen CT, Julien C, Bourasset F, Oddo S, LaFerla F, Bazinet RP, Calon F. 2009. Diffusion of docosahexaenoic and eicosapentaenoic acids through the blood-brain barrier: an in situ cerebral perfusion study. Neurochem Int 55:476–482. https://doi.org/10.1016/j.neuint.2009.04.018.
35. Spector R. 1988. Fatty-acid transport through the blood-brain barrier. J Neurochem 50:639–643. https://doi.org/10.1111/j.1471-4159.1988.tb02958.x.
36. Lee J, Ellis JM, Wolfgang MJ. 2015. Adipose fatty acid oxidation is required for thermogenesis and potentiates oxidative stress-induced inflammation. Cell Rep 10:266–279. https://doi.org/10.1016/j.celrep.2014.12.023.
37. Reamy AA, Wolfgang MJ. 2011. Carnitine palmitoyltransferase-1c gain-of-function in the brain results in postnatal microencephaly. J Neurochem 118:388–398. https://doi.org/10.1111/j.1471-4159.2011.07312.x.
38. Stoll EA, Makin R, Sweet IR, Trevelyan AJ, Miwa S, Horner PJ, Turnbull DM. 2015. Neural stem cells in the adult subventricular zone oxidize fatty acids to produce energy and support neurogenic activity. Stem Cells 33:2306–2319. https://doi.org/10.1002/stem.2042.
39. Schulz JG, Laranjeira A, Van Huffel L, Gartner A, Vilain S, Bastianen J, Van Veldhoven PP, Dotti CG. 2015. Glial beta-oxidation regulates Drosophila energy metabolism. Sci Rep 5:7805. https://doi.org/10.1038/srep07805.
40. Liu L, Zhang K, Sandoval H, Yamamoto S, Jaiswal M, Sanz E, Li Z, Hui J, Graham BH, Quintana A, Bellen HJ. 2015. Glial lipid droplets and ROS induced by mitochondrial defects promote neurodegeneration. Cell 160:177–190. https://doi.org/10.1016/j.cell.2014.12.019.
41. Lam TK, Pocai A, Gutierrez-Juarez R, Obici S, Bryan J, Aguilar-Bryan L, Schwartz GJ, Rossetti L. 2005. Hypothalamic sensing of circulating fatty acids is required for glucose homeostasis. Nat Med 11:320–327. https://doi.org/10.1038/nm1201.
42. Lam TK, Schwartz GJ, Rossetti L. 2005. Hypothalamic sensing of fatty acids. Nat Neurosci 8:579–584. https://doi.org/10.1038/nn1456.
43. Obici S, Feng Z, Arduini A, Conti R, Rossetti L. 2003. Inhibition of hypothalamic carnitine palmitoyltransferase-1 decreases food intake and glucose production. Nat Med 9:756–761. https://doi.org/10.1038/nm873.
44. Giusti SA, Vercelli CA, Vogl AM, Kolarz AW, Pino NS, Deussing JM, Refojo D. 2014. Behavioral phenotyping of nestin-Cre mice: implications for genetic mouse models of psychiatric disorders. J Psychiatr Res 55:87–95. https://doi.org/10.1016/j.jpsychires.2014.04.002.
45. Savonenko AV, Xu GM, Price DL, Borchelt DR, Markowska AL. 2003. Normal cognitive behavior in two distinct congenic lines of transgenic mice hyperexpressing mutant APPSWE. Neurobiol Dis 12:194–211. https://doi.org/10.1016/S0969-9961(02)00012-8.
46. Seibenhener ML, Wooten MC. 2015. Use of the open field maze to measure locomotor and anxiety-like behavior in mice. J Vis Exp 96:e52434. https://doi.org/10.3791/52434.
47. Kalueff AV, Stewart AM, Song C, Berridge KC, Graybiel AM, Fentress JC. 2016. Neurobiology of rodent self-grooming and its value for translational neuroscience. Nat Rev Neurosci 17:45–59. https://doi.org/10.1038/nrn.2015.8.
48. Savonenko A, Munoz P, Melnikova T, Wang Q, Liang X, Breyer RM, Montine TJ, Kirkwood A, Andreasson K. 2009. Impaired cognition, sensorimotor gating, and hippocampal long-term depression in mice lacking the prostaglandin E2 EP2 receptor. Exp Neurol 217:63–73. https://doi.org/10.1016/j.expneurol.2009.01.016.
49. Lee J, Choi J, Scafidi S, Wolfgang MJ. 2016. Hepatic fatty acid oxidation restrains systemic catabolism during starvation. Cell Rep 16:201–212. https://doi.org/10.1016/j.celrep.2016.05.062.
50. Lee J, Choi J, Selen Alpergin ES, Zhao L, Hartung T, Scafidi S, Riddle RC, Wolfgang MJ. 2017. Loss of hepatic mitochondrial long-chain fatty acid oxidation confers resistance to diet-induced obesity and glucose intolerance. Cell Rep 20:655–667. https://doi.org/10.1016/j.celrep.2017.06.080.
51. Chakravarthy MV, Zhu Y, Lopez M, Yin L, Wozniak DF, Coleman T, Hu Z, Wolfgang M, Vidal-Puig A, Lane MD, Semenkovich CF. 2007. Brain fatty acid synthase activates PPARalpha to maintain energy homeostasis. J Clin Invest 117:2539–2552. https://doi.org/10.1172/JCI31183.
52. Guzman M, Blazquez C. 2004. Ketone body synthesis in the brain: possible neuroprotective effects. Prostaglandins Leukot Essent Fatty Acids 70:287–292. https://doi.org/10.1016/j.plefa.2003.05.001.
53. Jones LL, McDonald DA, Borum PR. 2010. Acylcarnitines: role in brain. Prog Lipid Res 49:61–75. https://doi.org/10.1016/j.plipres.2009.08.004.
54. Wu R, Wu Z, Wang X, Yang P, Yu D, Zhao C, Xu G, Kang L. 2012. Metabolomic analysis reveals that carnitines are key regulatory metabolites in phase transition of the locusts. Proc Natl Acad Sci U S A 109:3259–3263. https://doi.org/10.1073/pnas.1119155109.
55. Szczepankowska D, Nałecz KA. 2003. Palmitoylcarnitine modulates palmitoylation of proteins: implication for differentiation of neural cells. Neurochem Res 28:645–651. https://doi.org/10.1023/a:1022802229921.
56. Leonardi R, Rock CO, Jackowski S, Zhang YM. 2007. Activation of human mitochondrial pantothenate kinase 2 by palmitoylcarnitine. Proc Natl Acad Sci U S A 104:1494–1499. https://doi.org/10.1073/pnas.0607621104.
57. McKenna MC, Scafidi S, Robertson CL. 2015. Metabolic alterations in developing brain after injury: knowns and unknowns. Neurochem Res 40:2527–2543. https://doi.org/10.1007/s11064-015-1600-7.
58. Brenna JT, Diau GY. 2007. The influence of dietary docosahexaenoic acid

and arachidonic acid on central nervous system polyunsaturated fatty acid composition. Prostaglandins Leukot Essent Fatty Acids 77:247–250. https://doi.org/10.1016/j.plefa.2007.10.016.
59. Brenna JT, Carlson SE. 2014. Docosahexaenoic acid and human brain development: evidence that a dietary supply is needed for optimal development. J Hum Evol 77:99–106. https://doi.org/10.1016/j.jhevol.2014.02.017.
60. Le Foll C, Dunn-Meynell AA, Miziorko HM, Levin BE. 2014. Regulation of hypothalamic neuronal sensing and food intake by ketone bodies and fatty acids. Diabetes 63:1259–1269. https://doi.org/10.2337/db13-1090.
61. Fernandez RF, Kim SQ, Zhao Y, Foguth RM, Weera MM, Counihan JL, Nomura DK, Chester JA, Cannon JR, Ellis JM. 2018. Acyl-CoA synthetase 6 enriches the neuroprotective omega–3 fatty acid DHA in the brain. Proc Natl Acad Sci U S A 115:12525–12530. https://doi.org/10.1073/pnas.1807958115.
62. Wolfgang MJ, Lane MD. 2011. Hypothalamic malonyl-CoA and CPT1c in the treatment of obesity. FEBS J 278:552–558. https://doi.org/10.1111/j.1742-4658.2010.07978.x.
63. Price NT, van der Leij FR, Jackson VN, Corstorphine CG, Thomson R, Sorensen A, Zammit VA. 2002. A novel brain-expressed protein related to carnitine palmitoyltransferase I. Genomics 80:433–442. https://doi.org/10.1006/geno.2002.6845.
64. Wolfgang MJ, Kurama T, Dai Y, Suwa A, Asaumi M, Matsumoto S, Cha SH, Shimokawa T, Lane MD. 2006. The brain-specific carnitine palmitoyltransferase-1c regulates energy homeostasis. Proc Natl Acad Sci U S A 103:7282–7287. https://doi.org/10.1073/pnas.0602205103.
65. Wolfgang MJ, Cha SH, Millington DS, Cline G, Shulman GI, Suwa A, Asaumi M, Kurama T, Shimokawa T, Lane MD. 2008. Brain-specific carnitine palmitoyl-transferase-1c: role in CNS fatty acid metabolism, food intake, and body weight. J Neurochem 105:1550–1559. https://doi.org/10.1111/j.1471-4159.2008.05255.x.
66. Lee J, Wolfgang MJ. 2012. Metabolomic profiling reveals a role for CPT1c in neuronal oxidative metabolism. BMC Biochem 13:23. https://doi.org/10.1186/1471-2091-13-23.
67. Wolfgang MJ, Lane MD. 2006. The role of hypothalamic malonyl-CoA in energy homeostasis. J Biol Chem 281:37265–37269. https://doi.org/10.1074/jbc.R600016200.
68. He W, Lam TK, Obici S, Rossetti L. 2006. Molecular disruption of hypothalamic nutrient sensing induces obesity. Nat Neurosci 9:227–233. https://doi.org/10.1038/nn1626.
69. Bowman CE, Zhao L, Hartung T, Wolfgang MJ. 2016. Requirement for the mitochondrial pyruvate carrier in mammalian development revealed by a hypomorphic allelic series. Mol Cell Biol 36:2089–2104. https://doi.org/10.1128/MCB.00166-16.
70. Eckel-Mahan KL, Patel VR, Mohney RP, Vignola KS, Baldi P, Sassone-Corsi P. 2012. Coordination of the transcriptome and metabolome by the circadian clock. Proc Natl Acad Sci U S A 109:5541–5546. https://doi.org/10.1073/pnas.1118726109.
71. Lee J, Choi J, Wong GW, Wolfgang MJ. 2016. Neurometabolic roles of ApoE and Ldl-R in mouse brain. J Bioenerg Biomembr 48:13–21. https://doi.org/10.1007/s10863-015-9636-6.
72. Brooks SP, Dunnett SB. 2009. Tests to assess motor phenotype in mice: a user's guide. Nat Rev Neurosci 10:519–529. https://doi.org/10.1038/nrn2652.
73. Park MJ, Aja S, Li Q, Degano AL, Penati J, Zhuo J, Roe CR, Ronnett GV. 2014. Anaplerotic triheptanoin diet enhances mitochondrial substrate use to remodel the metabolome and improve lifespan, motor function, and sociability in MeCP2-null mice. PLoS One 9:e109527. https://doi.org/10.1371/journal.pone.0109527.
74. Gilli F, Royce DB, Pachner AR. 2016. Measuring progressive neurological disability in a mouse model of multiple sclerosis. J Vis Exp 117:54616. https://doi.org/10.3791/54616.
75. Yang J, Li Q, Wang Z, Qi C, Han X, Lan X, Wan J, Wang W, Zhao X, Hou Z, Gao C, Carhuapoma JR, Mori S, Zhang J, Wang J. 2017. Multimodality MRI assessment of grey and white matter injury and blood-brain barrier disruption after intracerebral haemorrhage in mice. Sci Rep 7:40358. https://doi.org/10.1038/srep40358.
76. Zhao X, Wu T, Chang CF, Wu H, Han X, Li Q, Gao Y, Li Q, Hou Z, Maruyama T, Zhang J, Wang J. 2015. Toxic role of prostaglandin E2 receptor EP1 after intracerebral hemorrhage in mice. Brain Behav Immun 46:293–310. https://doi.org/10.1016/j.bbi.2015.02.011.
77. Zhang J, van Zijl PC, Mori S. 2002. Three-dimensional diffusion tensor magnetic resonance microimaging of adult mouse brain and hippocampus. Neuroimage 15:892–901. https://doi.org/10.1006/nimg.2001.1012.